MICROSCOPIC ANALYSIS OF ANEUPLOIDY INDUCED BY THE MUTATION OF THE CCDC124 GENE

by

ASMA ABDULLAH AL-MURTADHA

Submitted to the Graduate School of Engineering and Natural Sciences

in partial fulfillment of

the requirements for the degree of
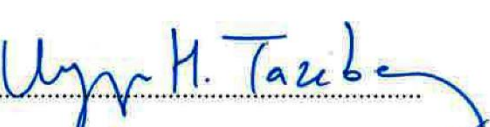
Master of Science

Sabancı University

December 2015

MICROSCOPIC ANALYSIS OF ANEUPLOIDY INDUCED BY THE MUTATION OF THE CCDC124 GENE

APPROVED BY:

Prof. Dr. Batu ERMAN ....
(Thesis Supervisor)

Prof. Dr. Selim ÇETİNER...

Prof. Dr. Uygar TAZEBAY...

DATE OF APPROVAL: 30/12/2015

ABSTRACT

MICROSCOPIC ANALYSIS OF ANEUPLOIDY INDUCED BY THE MUTATION OF THE CCDC124 GENE

ASMA ABDULLAH AL-MURTADHA

Molecular Biology, Genetics and Bioengineering, MSc. Thesis, 2015

Thesis supervisor: Batu Erman

Keywords: Ccdc124, HEK293T, Midbody, Centrosome, Confocal microscope

The Coiled-coil domain containing protein 124 (Ccdc124) is a centrosomal protein that relocates to the midbody region at the cytokinesis stage of the cell cycle. Cytokinetic abscission is the cellular process that leads to physical separation of two postmitotic sister cells by severing the intercellular bridge. Mutation of the Ccdc124 gene by CRISPR/Cas9 genome editing in HEK293T cells leads to the failure of cytokinesis and formation of aneuploid (multinucleated-MN) aberrant cells. In this study, the MN cells were analyzed using flow cytometry and confocal imaging followed by quantitative image analysis. MN cells had mitotic and chromosome attachment aberrations, multiple centrosomes and micronuclei. These aberrations are known to occur in tumour cells, a finding that links Ccdc124 to cancer. MN cells also upregulated the p53 protein, which induced senescence. Furthermore, MN cells had increased numbers of 53BP1 foci which indicates that the mutation of Ccdc124 induces the DNA damage response and activates the p53 pathway. This study documents a relationship between Ccdc124 mutation-associated cytokinesis failure and p53-dependent senescence.

ÖZET

CCDC124 GEN MUTASYON SONUCUNDA OLUŞAN ANÖPLYIDININ MIKROSKOPIK ANALIZI

ASMA ABDULLAH AL-MURTADHA

Moleküler Biyoloji, Genetik ve Biyomühendislik Programı, Yüksek Lisans Tezi, 2015

Tez Danışmanı: Batu Erman

Anahtar Kelimeler: Ccdc124, HEK293T hücre hattı, Midbody, Sentromer, Konfokal mikroskop

Hücre siklusunun sitokinez aşamasında çift kıvrımlı bölge içeren, "coiled coil domain containing" protein 124 (Ccdc124) sentromer bölgesinden midbody bölgesine taşınmaktadır. Midbody bölgesinde mitoz sonrası oluşan iki yavru hücrenin birbirinden ayrılması için hücreler arası köprünün koparılmasına sitokinetik kesilme (abscission) adı verilmektedir. HEK293T hücrelerinde CRISPR/Cas9 genom mühendisliği sonrasında Ccdc124 geninin mutasyonu sitokinez bozukluğuna ve anöplyidik çok çekirdekli ("MN") hücrelerin oluşmasına neden olmaktadır. Bu çalışmada bu MN hücreler akım sitometre, konfokal mikroskopik görüntüleme sistemleri ve kantitatif görüntü analizi ile çalışılmıştır. MN hücreleri mitotik ve kromozomal bağlanma bozuklukları, çoklu sentrozomlar ve mikro-çekirdekler içermektedir. Bu bozuklukların kanser hücrelerinde de sıklıkla görünmesi, Ccdc124 proteinini kanser ile ilişkilendirmektedir. MN hücrelerinin 53BP1 proteini içeren fokus sayılarında artış gözlemlememiz, Ccdc124 mutant hücrelerde DNA hasar yolaklarının ve p53 yolaklarının aktive olduğunu belirtmektedir. MN hücreleri buna bağımlı olarak p53 protein miktarını arttırmış ve p53 sinyalleri sonucunda ihtiyarlamış hücre tipine bürünmüşlerdir. Bu çalışma, Ccdc124 gen mutasyonu ile sitokinez bozuklukları ve p53 bağımlı hücre ihtiyarlaması arasında bir bağ kurmuştur.

To my family ….

ACKNOWLEDGEMENT

Firstly, I would like to express my sincere gratitude to my advisor Prof. Dr. Batu Erman for the continuous support of my master's study and related research, for his patience, motivation, and immense knowledge. His guidance helped me in all the time of research and writing of this thesis. I could not have imagined having a better advisor and mentor for my master's study.

Besides my advisor, I would like to thank my thesis jury members: Prof. Dr. Uygar Tazebay from Gebze Technical University for his precious support and great ideas for my project, and Prof. Dr. Selim Çetiner for his insightful comments and encouragement.

My sincere thanks also goes to Dr. Tolga Sütlü for his helpful ideas and comments. I also thank my friend Sinem Gül from Gebze Technical University for providing me with the necessary cell lines and antibodies for this project.

I thank my fellow labmates, Bahar Shamloo, Canan Sayitoğlu, Ahsen Özcan and my previous lab members Emre Deniz and Nazlı Keskin for their help and support. Also I thank my friends in Sabancı University Bahriye Karakaş, Ines Karmous, Amal Arachiche, also my dear friends Atia Shafique and Dilek Cakiroglu for their lovely company and continuous help.

Last but not the least, I would like to send my heartiest gratitude to all my friends and especially to my family in Yemen: my father Abdullah, my mother Kareema, my sisters Eqbal, Rahiq ,Eshraq and my brothers Ahmed and Mohammad for supporting me spiritually throughout my master's study and my life in general.

Finally, I would like to thank The Scientific and Technological Research Council of Turkey, TÜBİTAK BİDEB-2235 for the financial support during my master's education.

TABLE OF CONTENTS

TABLE OF FIGURES

LIST OF ABBREVIATIONS

γ	Gamma
bp	Base pair
Ccdc124	Coiled-coil domain containing protein 124
CIN	Chromosomal instability
CTCF	Corrected Total Cell Fluorescence
CRISPR	Clustered regularly-interspaced short palindromic repeats
DMEM	Dulbecco's Modified Eagle Medium
DMSO	Dimethylsulfoxide
DNA	Deoxyribonucleic Acid
EDTA	Ethylene diamine tetra acetic acid
FACS	Fluorescence Activated Cell Sorting
FBS	Fetal Bovine Serum
HCT	Human Colon Carcinoma
HEK	Human Embryonic kidney
IntDen	Integrated Density
MN	Multinucleated
MTOC	Microtubule organizing center
NL	Normal-looking
PCM	Pericentriolar material
PBS	Phosphate Buffered Saline
rpm	Revolution per minute
RNA	Ribonucleic Acid
ROS	Reactive Oxygen Species
SV40	Simian Virus 40
WT	Wild Type

1. INTRODUCTION

1.1. Cell Cycle and Mitosis

Eukaryotic cells that are actively dividing have to undergo a sequence of stages known as the cell cycle. The different stages of the cell cycle are two gap phases (G1 and G2); an S (for synthesis) phase, in which synthesis of DNA takes place and the number of chromosomes is duplicated; and an M (mitosis) phase, in which the genetic material and cytoplasm are divided. In the G1 phase, some metabolic changes occurs in the cell to prepare it for division. At a certain point the cell is ready to undergo division and proceed to the S phase where DNA synthesis takes place, which leads to the duplication of each chromosome as two sister chromatids. The G2 phase precedes mitosis, in which the cell undergoes metabolic changes leads to increase cell size and gathering of the cytoplasmic materials that are required for mitosis and cytokinesis stages. The G1, S and G2 stages are known as interphase. During mitosis, the cell undergoes nuclear material division (karyokinesis) which is followed by cytoplasm division (cytokinesis) (Fig.1.1).

The eukaryotic cells use mitosis as a process of the nuclear material division that happens when a parent cell divides to give rise to two daughter cells. The duration of mitosis in actively dividing eukaryotic cells takes approximately one hour. Mitosis indicates specifically the segregation of the duplicated chromosomes in the nucleus. Chromosomes are duplicated in the S phase and they are separated equally in which each daughter cell will contain one copy of all chromosomes. During mitosis the segregation of the genetic material (karyokinesis) is proceeded by a separation of the cell cytoplasm (cytokinesis) to give rise two identical daughter cells. Mitosis has different stages known as prophase, prometaphase, metaphase, anaphase, and telophase.
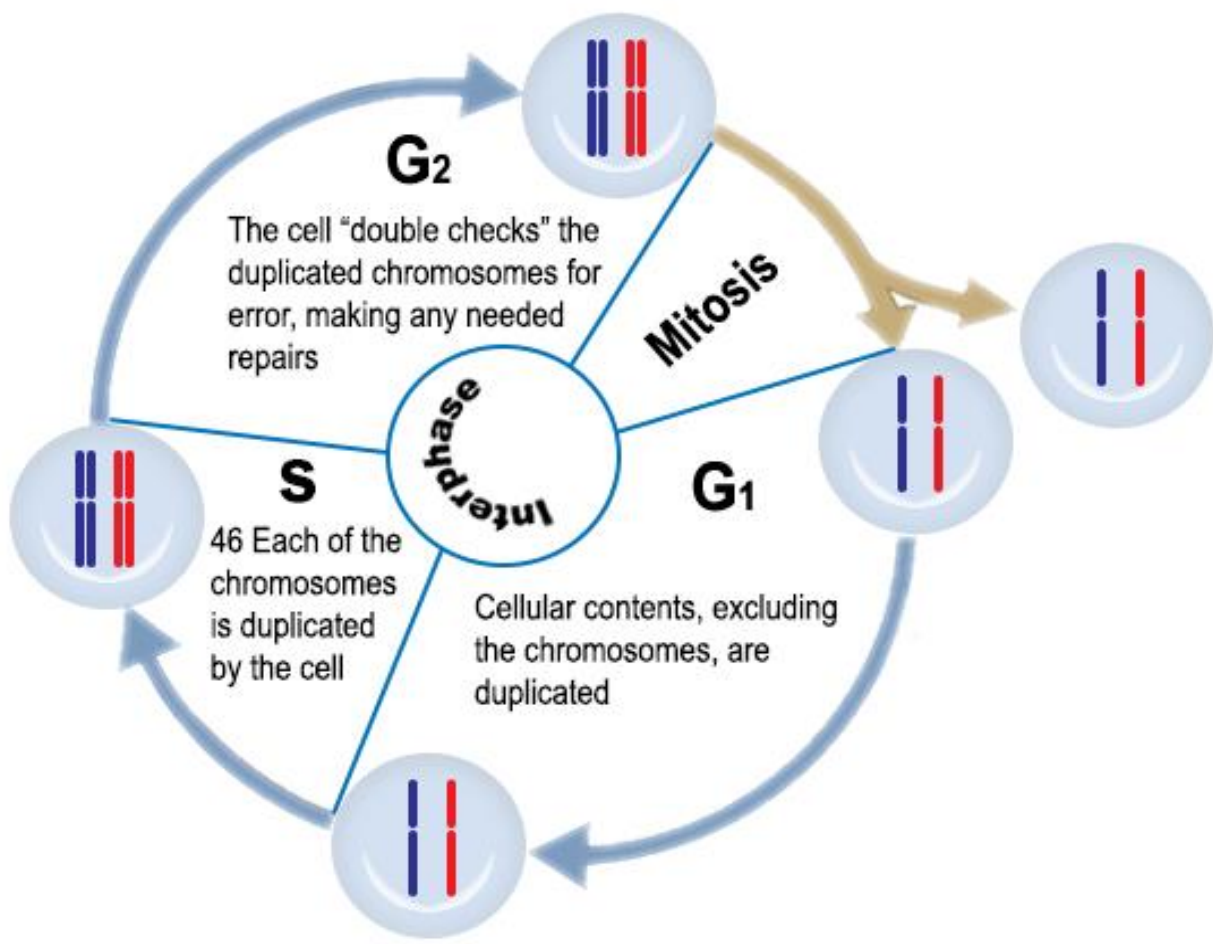
Figure 1.1 The cell cycle

The human genome contains 46 chromosomes (32 pairs) which are duplicated in the S phase (shown here are one representative pair of chromosomes in red and blue). Each chromosome is copied and each daughter cell receives one copy of each. The cell cycle contains two gap phases (G1 and G2) and S phase. The cell spends most of its life in G1, and is prepared to undergo mitosis. In S phase, DNA synthesis takes place which leads to the formation of sister chromatids for each chromosome. In the G2 phase, DNA undergoes another check to make any needed repair before entering mitosis. After this restriction point, the cell enter mitosis to divide the DNA and separate the cytoplasm in cytokinesis to form two daughter cells.

During prophase, the duplicated pairs of chromosomes undergo condensation and compaction process. Each pair of duplicated chromosomes is composed of two sister chromatids in which they are joined from a certain location that is called the centromere. Centrosomes start to migrate to each pole of the cell to form the mitotic spindles which are necessary for proper chromosome alignment and segregation.

During prometaphase, the nuclear membrane which surrounds the nucleus disintegrates and a protein structure is formed on each chromatid at the centromere which is called a kinetochore. After that, the microtubules that arise from each mitotic spindle extend from each pole to attach to the kinetochores in which each kinetochore should only be attached to one spindle pole. In metaphase, the microtubules start to pull the sister chromatids to ensure proper alignment at the center of the cell which is called the equatorial plane. The correct alignment ensures even segregation of the chromosomes during anaphase. Each sister chromatid is pulled to the opposite pole of the cell. Correct kinetochore-microtubule attachment guarantees that each daughter cell will receive same number of chromosomes. Finally, a cleavage furrow starts to separate the cytoplasm during telophase. The cytoplasm separation process is called cytokinesis which ends up with complete separation of the two daughter cells in an abscission process. A nuclear envelope forms around each set of chromosomes and they start to uncoil, to become diffuse and less compact in the nucleus (Fig.1.2).
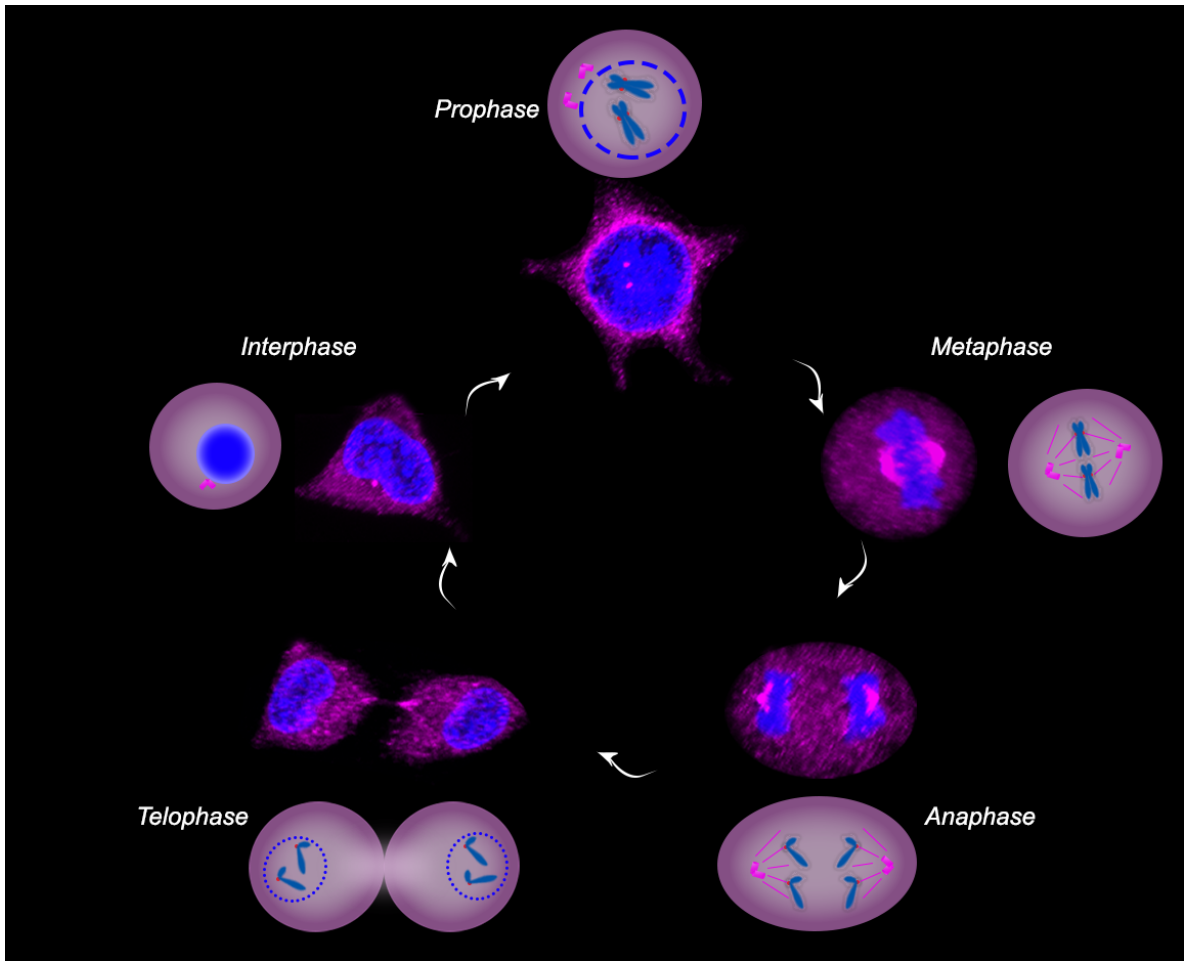
Figure 1.2 Stages of mitosis

Representative images of human kidney HEK293T cells obtained by confocal microscopy and stained with DAPI (in blue staining the DNA) and gamma tubulin, staining mostly the cytoplasm and the centrioles (in magenta). Dividing cells spend most of their lives in interphase and they enter mitosis after DNA synthesis in S phase. In the prophase stage, chromosomes condensation initiates and the centrosomes are duplicated (which can be seen as two dots in magenta color). In metaphase, chromosomes align in the middle of the cell and sister chromatids start to separate to opposite poles of the cell in anaphase. In telophase the two daughter cells separate and nuclear membrane start to reform.

1.2. The Centrosome

1.2.1. Centrosome Structure and Function

The centrosome is the primary microtubule-organizing center (MTOC) in the eukaryotic cells which regulates different cellular functions such as adhesion, cell motility, cellular polarity and organization of the spindle poles during mitosis. Many defects and abnormalities in the MTOC and mitotic spindle formation were identified to occur in different tumour types in which most of them were associated with genomic instability (CIN) because extra number and irregularities of the centrosomes can lead to abnormal cell division[1].

In the late 19th century, Boveri and van Beneden discovered the centrosome when they were studying cell division they noticed that the cells have a structure from which fibers emanated[2]. This structure replicated before mitosis and formed the two poles of the mitotic spindle[2]. The centrosome is comprised of two centrioles (described as mother and daughter centrioles) at right angles to each other and they are surrounded by an electron-dense matrix, the pericentriolar material (PCM). Each centriole has 9 microtubules (MTs) triplets that are organized in a symmetric 'cartwheel' structure. The centriole is ~0.5μm in length and 0.2μm in diameter and has appendages at the distal ends after maturation. This structure has other variations, in which triplets are substituted by singlets or doublets and no appendages are possible. The appendages dock cytoplasmic microtubules and might anchor and stabilize the centrioles to the cell membrane where they act as basal bodies[1,2].

Centriole characteristics define many properties of the centrosome for example its polarity, ability to replicate, dynamics and stability. The capacity of centrioles to replicate is essential for the duplication ability of the centrosome. Centrioles are highly stable structures, and their microtubules are resistant to temperature change and detergents. This stability might be a result of some post-translational modifications of the centiolar tubulin, such as polyglutamylation. The PCM organize nucleation and organization of the microtubules. The PCM and the centrosome do not have a membrane or boundary to determine their size or extent in the cell[1].

17

The PCM is composed of a network of 12–15 nm filaments with which the other proteins and elements bind. The size of PCM changes during the cell cycle and it reaches a maximum size at the metaphase–anaphase transition and a minimum size at telophase in most cells. Most of the known elements of the PCM have pools in both cytoplasm and centrosome, and the amount of these elements change in the centrosome which possibly happens by recruitment of materials from cytoplasm during cell division. One of the well-characterized elements of the PCM is a γ-tubulin ring complex. In the centrosome the γ-tubulin is a component of a large protein complex that forms an open ring structure that is around 25 nm in diameter, which is approximately the same diameter as a microtubule. The γ -tubulin rings act as a direct template for nucleation of microtubule. The PCM is not fully characterized and many elements are needed to be identified but some general components are becoming recognizable. For instance, different proteins of the PCM are largely predicted to have a coiled-coil structure such as pericentrin which is a large protein with coiled-coil structure that has been reported to form a dynamic reticular lattice in the PCM, and the Ccdc124 (coiled-coil domain containing protein) was characterized lately as a PCM protein which is discussed in more details in this study[1,2].

1.2.2. Centrosome Duplication

The centrosome does not have specific nucleic acids associated with it, so it must utilize some other procedure for replication. In the cell cycle during G1 phase, the cell has only one centrosome which composed of two (mother and daughter) centrioles and the surrounding pericentriolar material. The centrosome duplication process starts at the G1–S transition, at almost the same time of initiation of DNA replication procedure. The apparent characteristic of the centrosome is that the centrioles separate from each other. After separation, new daughter centrioles begin to form orthogonal to the mother centrioles. At G2, there are two centrosomes next to each other and each centrosome has a pair of centrioles within. Centrosome duplication is a semi-conservative process, in which each centrosome after duplication has one old (the mother) and one new centriole (the daughter). Typically, somatic cells should have a mother centriole to create a new daughter centriole,

even though, there are number of well-defined circumstances in both animal and plant cells in which the basal body or the centriole formation can occur *de novo*. The absence of a basic requirement for an existing centriole implies that new centrioles are not only templated by old or mother centrioles, and it is not identified yet how the structure of the centriole is propagated[1].

At the G2–M transition, the replicated centrosomes migrate to opposite sides of the nuclear membrane. This movement depends on the activity of kinesin microtubule motor proteins, especially those that act to slide apart anti-parallel microtubules. When the nuclear membrane breaks down, microtubules that arise from the centrosomes start to attach to the kinetochores of the chromosomes, and overlapped microtubules from the opposite poles, generate the bipolar mitotic spindle. Chromosomes segregation that is followed by cytokinesis leads to separation of two daughter cells with a single centrosome. In recent research, it was defined that cyclin E and its associated kinase Cdk2 are important for centrosome replication[3]. Cyclin E–Cdk2 reaches a maximum activity at the G1–S transition, and is also required for DNA replication initiation, consistent with the similar timing of these processes. Interestingly, the difference between DNA replication and centrosome duplication is that DNA replication has an extreme control that include a mechanism known as 'licensing', which relies on selective access of replication elements to the DNA. Centrosome duplication appears to be less strictly controlled, this idea is supported by previous identification of presence of multiple times of centrosome duplication in S phase within one cell cycle in both embryonic and somatic cells if cells were arrested artificially in S phase[1–3].

Bipolar spindle assembly

Pericentriolar material
(PCM)

M

G₂　　　G₁

S

Maturation and separation

Centriole disengagement

Duplication initiation
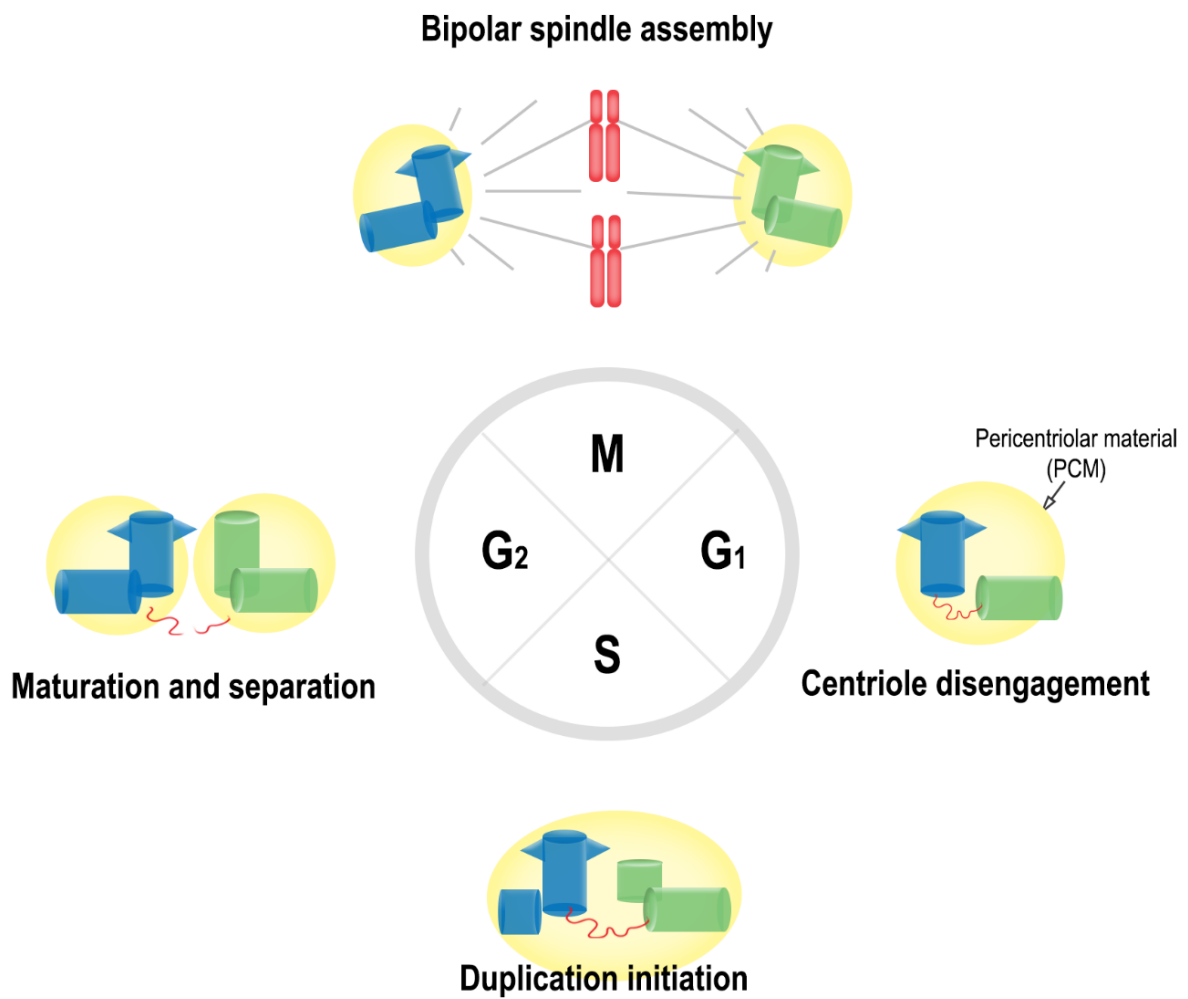
Figure 1.3 The centrosome duplication cycle

The centrosome cycle consists of several steps that are linked to the cell cycle. After cell division, each cell has one centrosome that contains two centrioles (green and blue) and the pericentriolar material (PCM) in yellow. Centriole disengagement occurs from the end of mitosis to early G1 phase and initiation of centriole duplication starts in S phase when a 'procentriole' (the shorter green and blue cylinders) forms at each centriole. These small procentrioles grow longer during the G2 phase and a PCM is formed around each centrosome then they separate to form two mature centrosomes. The separated centrosomes migrate to assemble the bipolar mitotic spindle (gray) during mitosis. The cell divides to make two cells that each contain one centrosome.

1.3. The Midbody

Midbody (or Flemming body) is a transient structure located in the intercellular bridge between two separating daughter cells during cytokinesis which is the final stage in cell division in which the abscission or severing of the intercellular bridge takes place to separate the two daughter cells from each other. Even though the midbody was discovered 100 years ago by Walther Flemming in 1891, its function is still not fully understood[4].

The midbody was found to locate to the site of abscission which physically separates two daughter cells[5]. It has a complex structure, it contains a tight bundle of antiparallel microtubules in its core and it contains several proteins such as cytoskeletal and other proteins. The midbody is formed from the midzone of an antiparallel bipolar microtubules that assembles between separating sister chromatids in anaphase (also called the central spindle).

Midzones between the separated sister chromatids forms the midbody during furrow ingression. The cleavage furrow is formed due to the assembly of a contractile actin–myosin ring which leads to compaction of the antiparallel midzone bundles into a single large microtubule bundle that forms the midbody core[6]. During compression, a bulge appears at the center of midbody which is called the stem body[5]. The midbody act as an anchor for the compressed cleavage furrow. Firstly, the ingressed furrow still include some elements of the contractile actin–myosin ring, that likely participates to its mechanical stability[6]. Midbodies are composed of microtubules that interact with proteins which colocalize to microtubules in the middle. It was identified that these proteins divide into three subgroups that relocate at several regions of the midbody which are the bulge, the dark zone, and the flanking zone[4].

The microtubules in the midbody undergo a posttranslational modification such as acetylation, these modifications are related to microtubules stability and resistance to different disturbances, for instance some depolymerizing drugs such as Nocodazole[7,8]. The microtubules' minus ends arise towards cytoplasmic regions that surrounds the nucleus, where they interact with gamma-tubulin[9,10]. Midbody microtubules undergo permanent growth both inwards and outwards the midbody [4]. As a result, gamma-tubulin relocalizes to the midbody region at the end of cytokinesis stage[10]. Additional to the condensed microtubules and surrounding plasma membranes, the midbody composed of a highly electron-dense material but its molecular elements are not fully characterized. Although the compressed appearance of the midbody, the interacting proteins inside can still spread and diffuse along the intercellular bridge and the midbody in all telophase and post-telophase stages[9,11].

The primary function of the midbody is to drive abscission, which in some previous studies was identified to be directed by the endosomal sorting complex required for transport (ESCRT) machinery and midbody break down by activity of some microtubule-severing proteins[10,12]. The mechanism that regulates the ESCRT machinery and severing proteins and their localization to the midbody region is unknown[5]. Following abscission, the midbody remnant attached to one of the postmitotic sister cells as shown in figure 1.4. These structures can be seen in immunofluorescence analysis of synchronized HEK293T which stained with anti-gamma tubulin (centrosome marker) and anti-Ccdc124 antibodies. Ccdc124 is a centrosomal protein that is recruited to midbody region at the end of telophase, the attached midbody remnant is shown in figure 1.5. The midbody remnant can stay attached to the one of the sister cells throughout several rounds of cell cycle in some cell types but in others it can be degraded by autophagy[10,13].
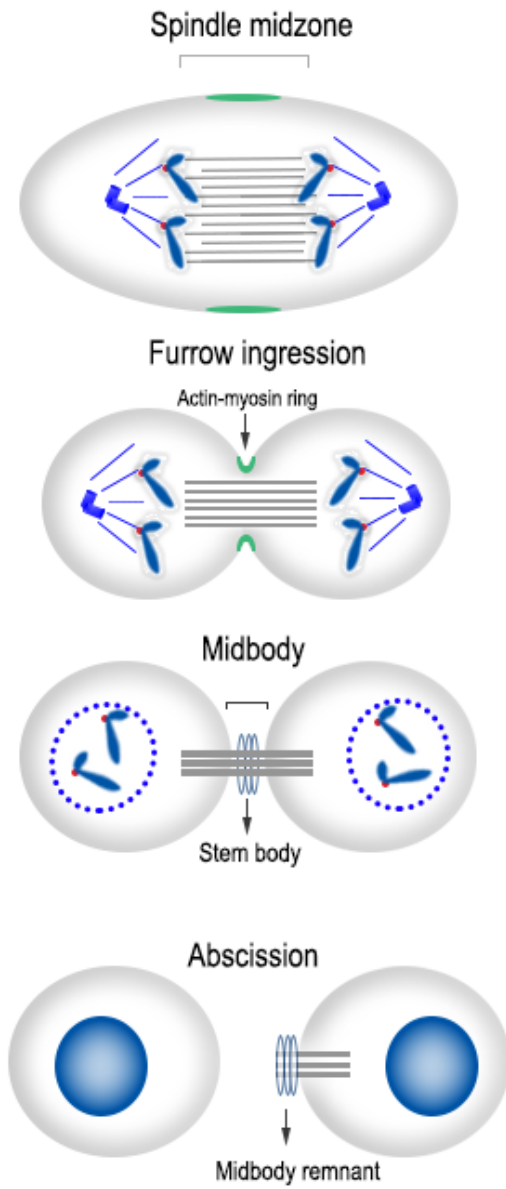
Figure 1.4 Midbody formation

During anaphase spindle midzone starts to form in the middle of the cell between separating sister chromatids which composed of antiparallel bundles of microtubules. After that, ingression furrow starts to form due to assembly of actin-myosin ring which compacts the midzone bundles to form a single large bundle that form the core of the midbody. During compaction a small bulge is formed in the middle of the midbody is called the stem body. After abscission, the remnants of the midbody usually inherited by only one of the separated two daughter cells.
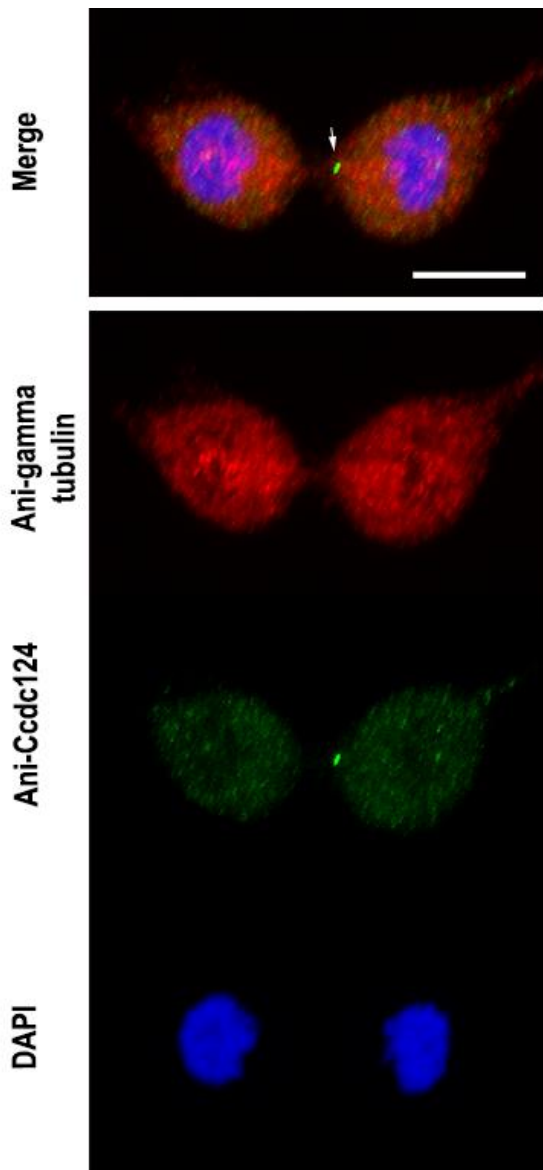
Figure 1.5 The midbody remnant

After abscission and separation, the midbody remnant is attached to one of the two daughter cells. Immunofluorescence was performed on HEK293T cells. They were arrested at the G_2/M phase by a double thymidine block followed by nocodazole treatment and then released for 60 minutes with fresh medium. Cells were immunostained using anti-gamma tubulin and anti-Ccdc124 antibodies. Both gamma-tubulin and the Ccdc124 are centrosome proteins and the Ccdc124 protein is recruited to the midbody region at cytokinesis. The arrowhead points to the midbody remnant which is attached to one of the newly separated daughter cells. The scale bar is 10μm.

1.4. The Ccdc124 Protein

1.4.1. Gene Structure

Coiled-coil domain containing protein 124 (Ccdc124) is an eukaryotic protein that is conserved from fungi-to-humans[14]. The Ccdc124 gene is located on human chromosome 19. The gene contains five exons and it has four known alternative transcripts. The first splice variant CCDC124-004 contains five exons, the first and part of the fifth exons are non-coding. This variant is translated to a protein of 223 amino acids. The second splice variant CCDC124-003 is a non-protein coding splice variant. The third splice variant CCDC124-001 is similar to the first variant and it is translated to a protein of 223 amino acids. The fourth splice variant CCDC124-002 does not have the last (fifth) exon and it is translated to a protein of 137 amino acids. The structure of the gene and the transcripts encoded by this gene can be seen in figure 1.6.

A recent study used northern blotting to identify the abundancy of Ccdc124 RNA in different human tissues and showed that Ccdc124 is a widely expressed gene in all tested human tissues, and it has a relative high levels of expression in the brain, placenta, liver, spleen, and prostate. Moreover, the Ccdc124 was identified as a 32kDa protein in immunoblots[14].

1.4.1. The Function of The Ccdc124 Protein

The Ccdc124 protein contains a coiled-coil domain (CCD) which is a conserved motif that is available in most centrosomal proteins, but its function is not well known yet. In a previous study, Ccdc124 protein was identified as a novel centrosome protein that is relocated to midbody region at telophase[14]. To identify Ccdc124 protein subcellular

localization, immunofluorescence assays were performed using Anti-Ccdc124 and Anti-gamma tubulin (centrosome marker) antibodies.
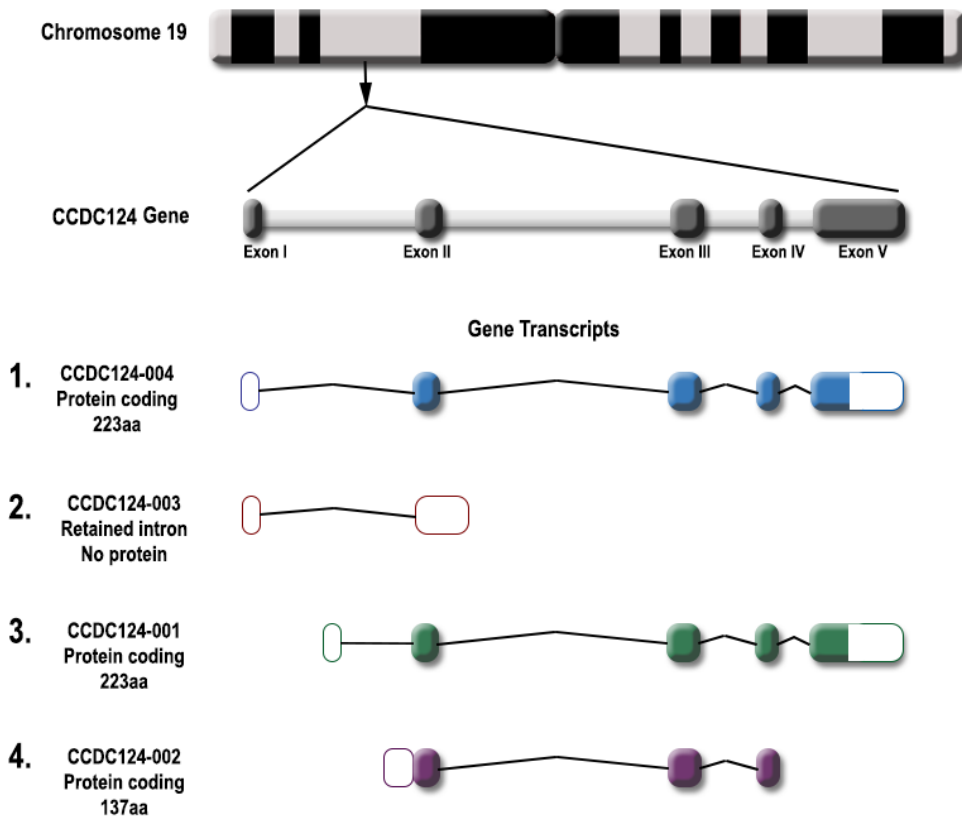
Figure 1.6 The Ccdc124 gene

The Ccdc124 gene is located in chromosome 19. It has five exons and four alternative splice variants, only three which are protein coding. The first and third splice variants are translated to a protein of 223 amino acids and the fourth variant is translated to a protein of 137 amino acids. Empty boxes represent non-coding exons while filled boxes represent protein coding exons.

Subcellular dot-like structures were observed during interphase in non-synchronized cells. After cell synchronization in the G2/M phase by double thymidine block followed by nocodazole treatment (a microtubule polymerization inhibitor), Ccdc124 protein was colocalized with gamma-tubulin at prophase where two dot-like structures were observed after centrosome replication. Staining for Ccdc124 was more diffuse and mostly localized

at the spindle poles of cells that were scored to be in metaphase and anaphase. In cells that were scored to be in telophase and cytokinesis, Ccdc124 protein dissociated from centrosome and relocated in the intercellular bridge at the midbody region between the two daughter cells. These observations were originally made in human cervical carcinoma, HeLa cells by Prof. Dr. Uygar Tazebay's laboratory and replicated in the human kidney cell line HEK293T (Fig. 1.7) [14].

To assess the important role of the Ccdc124 protein during cell separation, a previous study knocked down Ccdc124 by transfecting HeLa cells either with esiRNAs or with shRNA vectors which particularly targeting this gene. Knockdown efficiencies indicated approximately a 75–80% decrease in Ccdc124 levels in cells that received gene specific esiRNAs as compared to scrambled shRNA controls. The analysis of the cell morphology, centrosome localization and midbody functions in asynchronous growing cells were shown to be defective. Immunostaining of Ccdc124 knock-down cells demonstrated that centrosomes were formed in interphase, which indicate that Ccdc124 does not have an effect on centrosome formation. However, the importance of Ccdc124 was obvious during cytokinesis in which multinucleated cells were observed[14].

Furthermore, similar results were observed when the Ccdc124 gene was mutated by the CRISPR/Cas9 genome editing system in HEK293T cells[15]. The Ccdc124 gene has one translation initiation site (TIS) at the beginning of exon II and another TIS before exon III, so to knock out both the long and the shorter proteins, the mutation targeted exon III of Ccdc124 gene[16]. Sequence analysis of single cell cloned mutant cells revealed deletions and insertions in exon III of the Ccdc124, one clone, named H60, demonstrated a dramatic multinucleated cell phenotype -was used for further study in this thesis-. The mutation in the H60 clone caused a 91 nucleotide deletion in the first allele and a 24 nucleotide deletion in the second allele in the Ccdc124 gene (Fig. 1.8).

Previous studies by the Tazebay laboratory found that the Ccdc124 protein interacts with the Ras guanine nucleotide exchange factor RasGEF1B[14]. The RasGEF1B was firstly demonstrated in zebrafish as a protein that is expressed in nerve cells during late embryogenesis and early larval stages[17]. In addition, RasGEF1B was identified to be an exchange factor that activates specifically the small G protein Rap2[18].
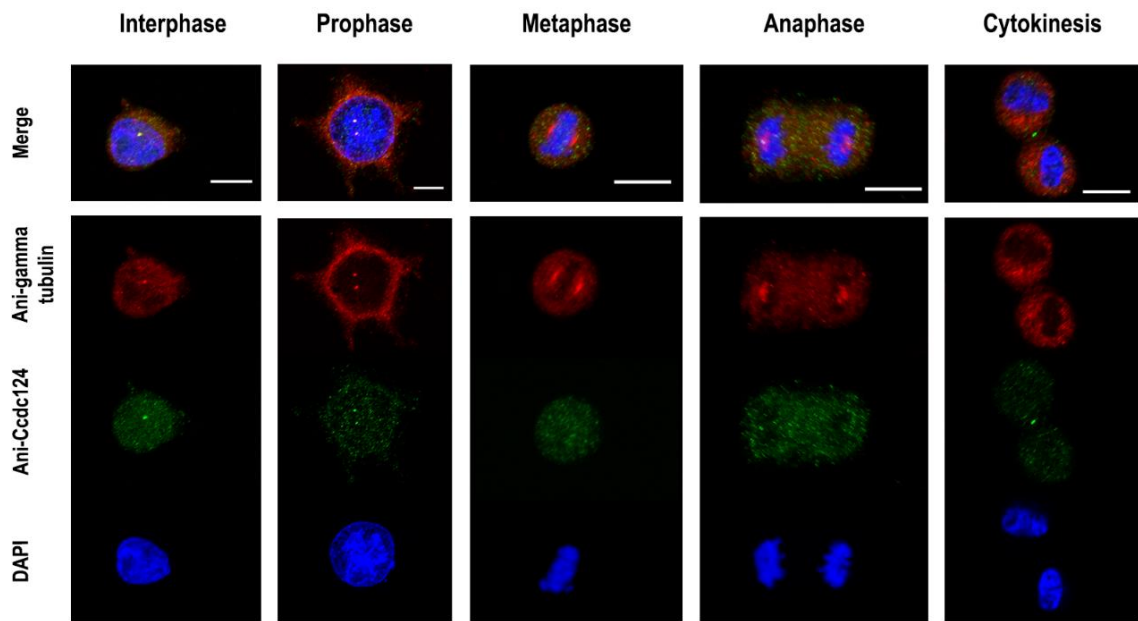
Figure 1.7 Ccdc124 protein subcellular localization during mitosis

HEK293T cells were arrested at the G_2/M phase by double thymidine block and nocodazole treatment. The cells were released from this block by washing the drug and adding a fresh medium. Cells were analyzed by immunofluorescence at 0, 15, 30 and 45 minutes after release from the cell cycle block. Anti-mid-Ccdc124 rabbit polyclonal antibody staining is shown in green, anti-gamma tubulin mouse monoclonal antibody staining is shown in red and DAPI staining is shown in blue. The scale bar is 10 μm.

Furthermore, RasGEF1B was demonstrated in murine macrophages as a toll-like receptor inducible protein in which it localized in early endosomal vesicles[19]. RasGEF1B was identified to locate in endosomal vesicles and this was shown by using fluorescent tagged-proteins of the RasGEF1B such as YFP-RasGEF1B or mRFP-RasGEF1B in CHO cells[19]. Characterization of RasGEF1B which is an endosomal vesicle factor as an interaction partner of centrosomal and/or midbody Ccdc124 protein is important because endosomes were demonstrated to have a role in the severing process on intercellular bridge during cytokinetic abscission[20]. In a separate study, RasGEF1B was localized at a pericentrosomal/centrosomal position in metaphase cells, which is similar to the subcellular localization of Ccdc124[14]. In addition, the same localization of both proteins was observed at telophase and during cytokinesis at the intercellular bridge and in the midbody. RasGEF1B was obviously colocalized with Ccdc124 at the midbody region, which indicate
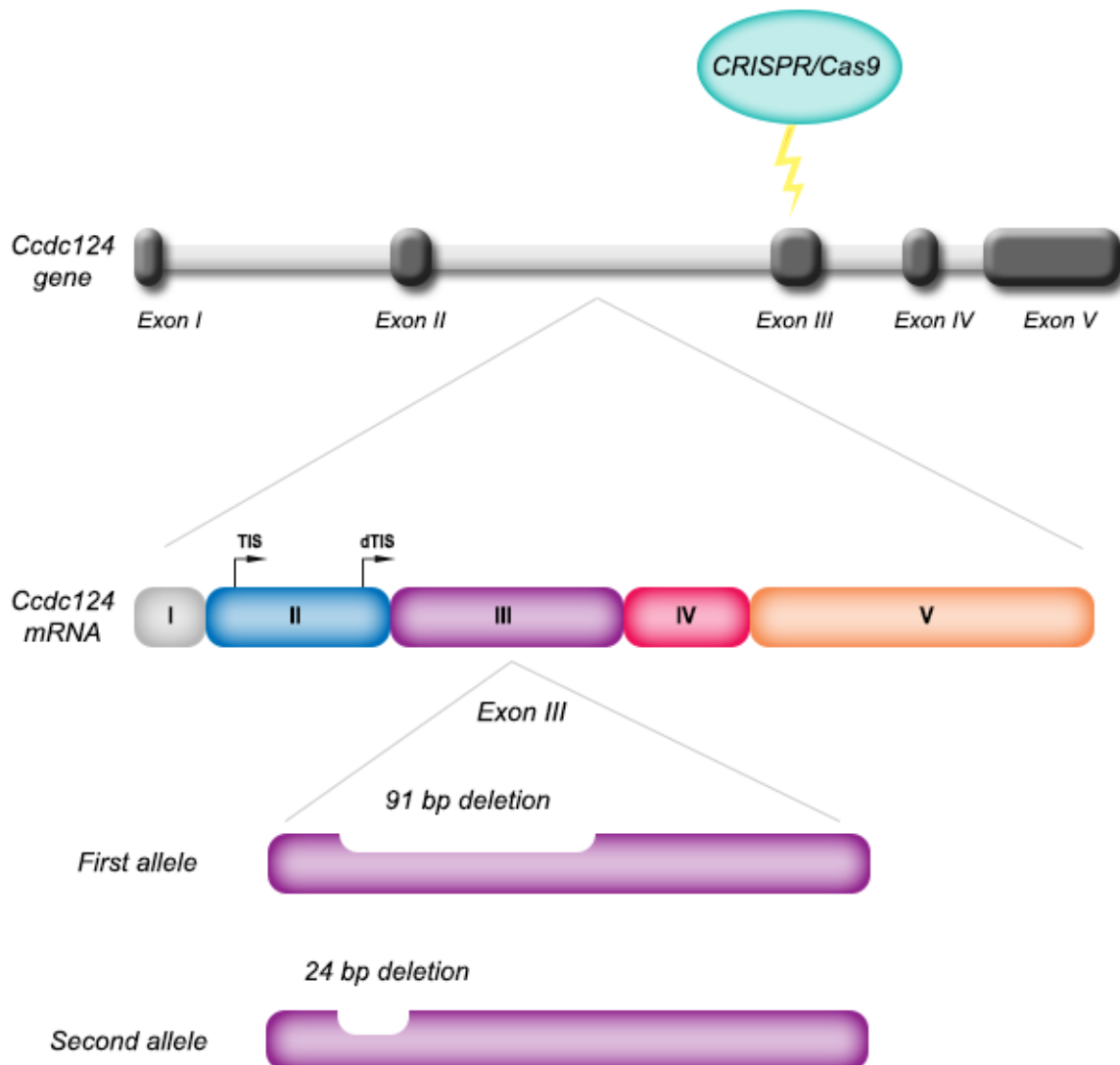
Figure 1.8 Ccdc124 gene mutation in the H60 clone

Ccdc124 gene was mutated using CRISPR/Cas9 technique that targeted exon III to knockout the known protein isoforms of the Ccdc124 protein. Sequencing results revealed that the gene is mutated in exon III and 2 different mutations were observed. In the first allele a 91 nucleotide deletion and in the second allele a 24 nucleotide were observed.

that the midbody forms an interaction site for the two proteins in late cytokinesis stage. These findings suggest a possible function of Ccdc124 that links cytokinesis to the unidentified RasGEF1B dependent signaling at the midbody. In addition, Ccdc124 does not modulate the activity of RasGEF1B[14].

This thesis follows up on the work of Sinem GÜL from Prof. Dr. Uygar Tazebay from Gebze Technical University, analyzing the effects of the mutation of the Ccdc124 gene in the H60 clone of CRISPR/Cas9 genome edited HEK293T human kidney cells. The present study extensively uses confocal microscopy to analyze the defects in the various stages of the cell cycle in these mutant cells in detail. We identified for the first time that mutation of Ccdc124 results in defects of cytokinesis which results in cellular stress, upregulation of the tumor suppressor protein p53 and induces cellular senescence. Curiously these phenotypes are observed only in the multinucleated cells of the H60 clone, while normal looking cells which share the same genotype as the multinucleated cells do not display this phenotype. Speculations about the product precursor relationship between the normal looking and multinucleated cells in the H60 clone are made in the discussion section of this thesis (Fig.4.1).

2. MATERIALS AND METHODS

2.1. Materials

2.1.1. Chemicals

2.1.1.1. Cell cycle synchronization chemicals

- Nocodazole was dissolved in DMSO to make 10mg/ml stock solution. 50ng/µl was used as working dilution.

- Thymidine was dissolved in ddH$_2$O to make 100mM stock solution. 2mM was used as working dilution.

2.1.1.2. Senescence associated β-galactosidase assay chemicals

- Potassium Ferricyanide was dissolved in ddH$_2$O to make 5mM stock solution (3.3g/50ml).

- Potassium Ferrocyanide was dissolved in ddH$_2$O to make 5mM stock solution (4.2g/50ml).

- MgCl$_2$ was dissolved in ddH$_2$O to make 2mM stock solution (2 g/50ml).

- NaCl was dissolved in ddH$_2$O to make 150mM stock solution (17.5 g/50ml).

- X-gal was dissolved in DMSO to make 50mg/ml.

- Citric acid was dissolved in ddH$_2$O to make 0.1M stock solution (19.2 g/L).

- Sodium phosphate heptahydrate was dissolved in ddH$_2$O to make 0.2M stock solution (53.6 g/L).

The rest of the chemicals used in this project are listed in the Appendix A.

2.1.2. Equipment

All equipment used in this project are listed in the Appendix B.

2.1.3. Buffers and Solutions

2.1.3.1. Immunofluorescence staining solutions

- Blocking solution: 1% BSA in 1X PBS and 10% goat serum.

- Antibody dilution solution: 0.5% 100 Triton X – 100 with 1% BSA in 1X PBS

2.1.3.2. Propidium Iodide (PI) staining solutions

- Propidium iodide (1mg/ml), 60µl Triton X-100 and 100µl RNAse (stock: 10mg/ml) and the volume was adjusted to 10 ml with cold FACS incubation buffer.

- FACS incubation buffer (pH: 7.4): 10mM HEPES, 140mM NaCl and 2.5mM CaCl$_2$.

2.1.3.3. Senescence assay staining solutions

- Staining solution:

250µl of 200mM Potassium Ferricyanide , 250µl of 200mM Potassium Ferrocyanide, 100µl of 200mM MgCl2, 250µl of 6M NaCl and 200µl of 50mg/ml X-gal in DMSO were added to 10ml of the citric acid/sodium phosphate buffer.

- Citric acid/sodium phosphate buffer for the staining solution (pH:6):

39.4ml of 0.1M citric acid, 60.6ml of 0.2 M sodium phosphate heptahydrate was added to 100ml of ddH$_2$O.

2.1.3.4. Mammalian cell culture buffers and solutions

- Phosphate-buffered saline (PBS): Commercial Dulbecco's Phosphate Buffered Saline 10X were used.

- Trypan blue dye (0.4% w/v): 40µg of trypan blue was dissolved in 10ml PBS.

2.1.4. Tissue Culture Growth Media

- Growth media for adherent cell lines: HEK 293T and HeLa cell lines were grown in filter-sterilized Dulbecco's Modified Eagle Medium (DMEM) that is supplemented with 10% heat-inactivated fetal bovine serum, 2mM L-Glutamine, 100 unit/mL penicillin and 100 unit/mL streptomycin.

- Freezing Medium: All the cell lines were frozen in medium containing Dimethyl sulphoxide (DMSO) added into fetal bovine serum (FBS) at a final concentration of 10% (v/v) and stored at 4°C.

2.1.5. Tissue Culture Cell Lines:

- HEK293T (derivative of human embryonic kidney 293 cell line that stably express the large T antigen of SV40 virus were obtained from laboratory stocks were used in immunofluorescence, subcellular localization, quantification and FACS experiments.

- H60 (Ccdc124 mutated clone of HEK293T that contain multinucleated cells that fails to undergo normal mitosis) was used in immunofluorescence, subcellular localization and fluorescence quantification experiments.

- Human colon carcinoma cell lines HCT116 were used as positive controls in immunofluorescence and quantification experiments.

2.1.6. Antibodies

Primary antibodies, secondary antibodies and stains used in immunofluorescence experiments with working dilutions are listed in Table 2.1

Antibody	Working dilution	Company
CCDC124 Antibody Rabbit Polyclonal	1:1000	Bethyl Laboratories, Inc.
Anti-gamma Tubulin primary antibody [GTU-88] - Centrosome Marker	1:1000	Abcam
P53 (1C12) Mouse mAb (Alexa Fluor 488 Conjugate)	1:500	Cell Signaling Technology
Goat anti-Mouse IgG (H+L) Secondary Antibody, Alexa Fluor® 555 conjugate	1:2000	ThermoFisher SCIENTIFIC
DyLightTM 488 – Labeled Antibody to Rabbit IgG (H+L)	1:2000	KPL, Inc.
DAPI (4′,6-Diamidino-2-phenylindole dihydrochloride)	1:1000 of 1mg/ml stock solution	Roche Diagnostics GmbH
Alexa Fluor 555 Phalloidin	1:200	ThermoFisher SCIENTIFIC

Table 2.1 Primary and secondary antibodies used in Immunofluorescence experiments

2.1.7. Software and Computer Programs

The software and computer based programs used in this project are listed in Table 2.2

Program Name	Website/Company	Use
ImageJ	Open source, Java-based image processing program developed at the National Institutes of Health NIH.	View, analyze confocal images and fluorescence quantification measurements.
ZEN 2009 Light Edition	Carl Zeiss Inc.	View and analyze confocal microscope data
FlowJo 7.6.1	Tree Star Inc.	View and analyze flow cytometry data
Adobe Photoshop	Adobe Systems Incorporated	Image design
Adobe Illustrator	Adobe Systems Incorporated	Graphs and images design.

Table 2.2 Software and computer programs used in this project

2.2. Methods

2.2.1. Mammalian Cell Culture

Maintenance of Adherent Cells: Adherent cells used in this project were HEK293T derived clones and the HCT116 colon cancer cell line. These cells were grown in filter-sterilized DMEM that was supplemented with 10% heat-inactivated fetal bovine serum, 2mM L-Glutamine, 100unit/mL penicillin and 100unit/mL streptomycin in 10mm tissue culture plates in a 37ºC, 5%CO_2 incubator. When the plate reached to 70-80% confluency, cells were split into pre-warmed, fresh medium with a ratio of 1:10. Adherent cells were trypsinized before splitting as described below.

Trypsinization: Adherent cells were trypsinized to detach the cells both from the plate and from each other. After removing the old medium, plates were washed with serum free DMEM or 1X PBS to remove the serum to prevent inactivation of the trypsin enzyme.

2mL of prewarmed (37° C) trypsin solution was added on the plate and incubated until the cells were detached from the plate (approximately 2 minutes) at 37°C. 8 mL of fresh medium containing serum was then added to the trypsin on the plate surface and cells were mixed and harvested to a 15 mL falcon tube. After centrifugation at 1000 rpm for 5 minutes, the medium was removed and cells were resuspended in pre-warmed fresh DMEM that was supplemented with 10% heat-inactivated fetal bovine serum, 2mM L-Glutamine, 100 Units/mL penicillin and 100 Units/mL streptomycin for further incubation.

Cell Freezing: After trypsinization 10^6 cells were centrifuged at 1000 rpm for 5 minutes and the medium was removed. The cells were resuspended in 1 mL ice-cold freezing medium containing DMSO added into fetal bovine serum (FBS) at a final concentration of 10% (v/v) and were pipetted in cryo vials. They were stored at -80°C in a cryobox for 24-48 hours and were then transferred to the liquid nitrogen tank.

Cell Thawing: Frozen cells in cryo vials were resuspended in 10mL complete growth medium in a 15mL falcon tube. The cell suspension was centrifuged at 1000 rpm for 5 minutes. After removing the supernatant, the cells were resuspended in 10mL prewarmed fresh complete medium and transferred to either plates or flasks.

2.2.2. Coverslips Sterilization and Coating with Poly L-lysine

The coverslips used in this project were 18 X 18 mm in diameter, size 1.5, 0.17 +/-0.0001 micrometer thickness. The coverslips were soaked in 70% ethanol overnight then dried and autoclaved for 20 minutes/121^{0}C. The sterile coverslips were soaked in a poly L-lysine (filter sterilized) solution for 5 minutes then washed twice with sterile ddH$_2$O and left to dry in the tissue culture hood for 1 hour.

2.2.3. Cell Cycle Synchronization

2.2.3.1. Double Thymidine block with Nocodazole

Cells were cultured over autoclave sterilized poly-L lysine coated coverslips in 3.5 cm^2 or 6-well plate. Approximately $2x10^5$ cells/well were seeded and incubated in a tissue culture incubator, until they were 70% confluent. Cells were synchronized by a first thymidine block (2 mM) for 16 hours. Cells were washed with 1X PBS twice, fresh culture medium was added to release cells from growth arrest for 8 hours. The cell cycle was blocked a second time with thymidine (2 mM) for an extra 16 hours. Cells were washed with 1X PBS twice, followed by 50ng/µl nocodazole treatment for 12 hours. Arrested cells were fixed, and analyzed either directly, or washed twice with 1XPBS and re-cultured in fresh medium for 15, 30, 45, 60, or 90 minutes, and at each time point cells were processed for immunofluorescence.

2.2.3.2. Nocodazole synchronization

Cells were cultured over poly-L lysine coated coverslips. Approximately $2x10^5$ cells/well were seeded and incubated in a tissue culture incubator until they were 70% confluent. Cells were synchronized by treating with Nocodazole (50ng/µl) containing complete DMEM and culturing in the tissue culture incubator for 15 hours. Arrested cells were fixed, and analyzed either directly, or washed twice with 1XPBS and re-cultured in fresh medium for 15, 30, 45, 60, or 90 minutes, and at each time point cells were processed for immunofluorescence.

2.2.4. Immunofluorescence Experiments

Before seeding cells, Poly-L-lysine coated coverslips were attached to the surface of 6-well plates then $2x10^5$ cells were seeded in each well and incubated in 37^0 C for approximately 24 hours and were processed for immunofluorescence.

2.2.4.1. Subcellular localization of the Ccdc124 protein

After the aforementioned incubation period and cell cycle arrest periods, growth medium was removed from plates and the cover slips were washed twice with 1X PBS. Cells were fixed for 10 minutes in room temperature with 100% methanol cooled to -20C^0, then washed twice with 1X PBS. Next, Cells were permeabilized for 10 minutes in PBS with 0.5% Triton X-100 followed by two rounds of a 1XPBS. Cells were blocked for 1 hour at room temperature with blocking solution (PBS with 1% BSA and 10% goat serum) 200 μl for each coverslip.

Primary antibodies (Ccdc124 rabbit polyclonal antibody and gamma-Tubulin mouse monoclonal antibody) were diluted in blocking solution (1:1000 dilution) and 50 μl was added dropwise onto each coverslip and incubated in the dark for 2 hours at room temperature, followed by 4 washes (5 minutes each) with 1% BSA in 1X PBS.

Coverslips were incubated in the dark for 1hour at room temperature with secondary antibodies 50 μl (Goat anti-Mouse IgG (H+L) Secondary Antibody - Alexa Fluor® 555 conjugate and DyLightTM 488 – Labeled Antibody to Rabbit IgG (H+L)) diluted in blocking solution (1:2000 dilution) followed by 4 washes (5 minutes each) with 1% BSA in 1X PBS.

To stain cells nuclei, coverslips were incubated with 1μg/mL DAPI (4',6-Diamidine-2'-phenylindole dihydrochloride) solution for 5 minutes in dark at room temperature, followed by 2 washes with 1X PBS. Coverslips were mounted on glass slides with ProLong Gold Antifade (Invitrogen) mounting medium. Coverslips were left to dry at room temperature in the dark and were sealed onto microscope slides with transparent nail polish. Cells were visualized using the *Zeiss LSM 710* inverted confocal microscope with 63x/1.4 *oil immersion objective.*

2.2.4.2. P53 protein immunofluorescence staining

Protocol in 2.2.3.1 was used in this experiment, except fixation was made with warm 4% Paraformaldehyde (Pfa) for 20 minutes at room temperature. As a primary antibody, p53 (1C12) Mouse mAb (Alexa Fluor 488 Conjugate) was used at a 1:500 dilution.

2.2.5. Propidium Iodide Staining for Cell Cycle Analysis with Flow Cytometry

10^6 cells were used for flow cytometric analysis. Cultured cells were harvested with trypsin (0.05% Trypsin/0.53 mM EDTA) then centrifuged at 1000 rpm in a Sorvall tabletop centrifgure (model number) at room temperature for 5 minutes. The supernatant was removed and the cells were washed twice with ice cold 1X PBS. After the second wash supernatant was removed and cells resuspended again in the tubes and fixed with 70% ice cold ethanol dropwise by mixing with a vortex mixer and incubated for 15 minutes at room temperature, followed by one wash with ice cold 1X PBS. 200 µl of Propidium iodide (PI) staining buffer was added to each tube to stain DNA and incubated in the dark for 45 minutes at room temperature. Cells were resuspended in 500µl of FACS buffer. The flow cytometric analysis of the cells was performed on a Beckton Dickenson BD FACSCanto flow cytometer. PI was excited by the argon laser at 488nm and fluorescence was detected in the PE-A channel. Results were analyzed with Flowjo software.

2.2.6. Confocal Microscopy Image Acquisition

The Ziess Zen 2010 software was used to acquire Z stacks and tile scans images. The 488nm Argon laser was used for excitation of Alexa Fluor 488, the 561nm laser was used for excitation of Alexa Fluor 555 and the 405nm UV laser was used for excitation of DAPI. ImageJ software was used to generate maximum intensity projection images of the Z stacks and to analyze and process images saved as .tiff files.

2.2.7. Quantification of P53 Protein Fluorescence

ImageJ was used to select DAPI stained nuclei from maximum intensity projection images. After splitting channels, a threshold was used to select nuclei and an 8bit image was created. All selections were saved in ROI manager in Imagej and transferred to the green channel of tiff files containing the p53 fluorescence. All measurements (Area, IntDen, Mean gray value and Raw IntDen) were made on these .tiff files and quantified in ImageJ software (Fig.2.1).
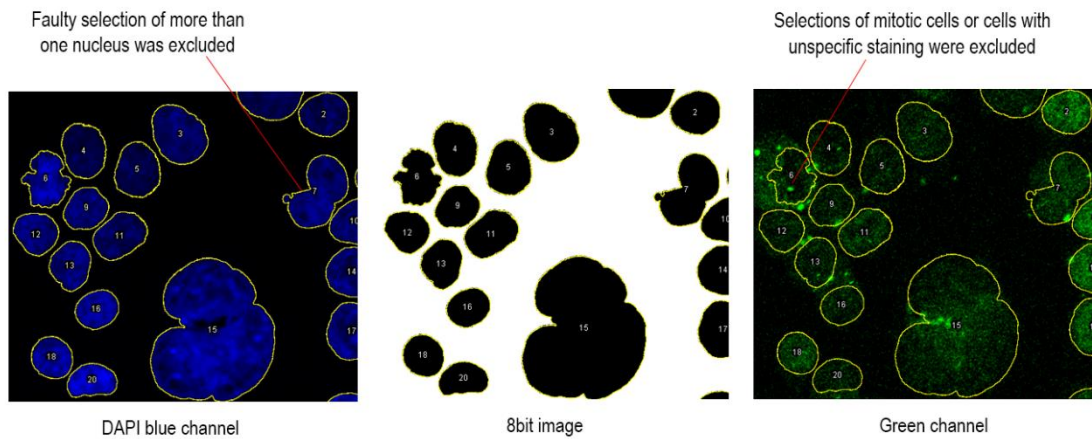
Figure 2.1 Selection of nuclei by ImageJ for quantification experiments

The DAPI blue channel was firstly used to select cell nuclei. A threshold was used to create black and white 8bit images. All selections were saved in ROI manager as a zip file and these selections transferred to the green channel of .tiff files containing p53 protein fluorescence.

Measurements were calculated by ImageJ software (Fig. 2.2). Area of the selection was measured in μm^2. Integrated Density (IntDen) was calculated by multiplying the mean fluorescence gray value by the area. Mean gray value is the sum of the gray values of all the pixels in the selection divided by the number of pixels. Area and IntDen were used for all quantification procedures.

Area	Mean	IntDen	RawIntDen
362.658	37258.664	13512166.146	1705180013.000
252.298	40627.165	10250160.795	1293528301.000
470.198	38990.615	18333290.262	2313586126.000
846.818	38834.913	32886115.046	4150092996.000
432.383	41260.210	17840225.199	2251363335.000
967.765	37245.126	36044535.267	4548672689.000
729.873	40909.261	29858571.054	3768029347.000
724.786	39218.329	28424888.239	3587104449.000
647.945	41519.837	26902569.551	3394994067.000
1520.620	42768.479	65034599.040	8207099975.000
354.417	39953.458	14160193.132	1786958364.000
594.718	38348.706	22806673.169	2878108723.000
347.967	37728.377	13128227.312	1656728505.000
906.583	40980.695	37152382.062	4688478416.000
358.554	37185.587	13333027.343	1682573430.000
569.820	40500.199	23077839.451	2912328797.000
251.775	38344.392	9654167.280	1218316361.000
425.727	37809.232	16096409.773	2031300972.000
263.455	39692.910	10457313.946	1319670180.000
280.326	38148.038	10693889.169	1349525004.000
369.457	43724.007	16154154.238	2038588087.000
524.510	36568.240	19180403.608	2420488360.000
280.382	39276.530	11012413.399	1389721457.000
401.970	45270.098	18197233.008	2296416258.000
171.590	38610.298	6625154.865	836067403.000
234.421	37248.121	8731750.665	1101911163.000
416.416	40037.251	16672154.223	2103957563.000
281.737	36652.472	10326341.326	1303141972.000

Figure 2.2 Calculations of measurements by ImageJ for p53 protein fluorescence
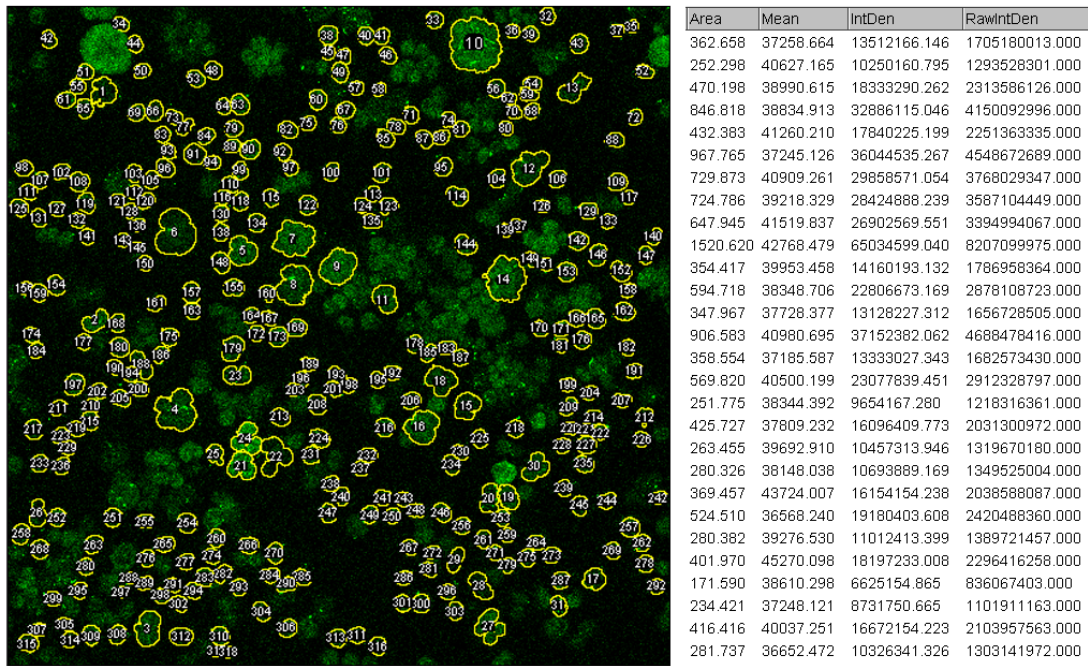
All experiments with fluorescence quantification were generated by calculating the (Area, Mean gray value, IntDen, and Raw IntDen) for each selected nucleus area.

To calculate the background fluorescence, 10 measurements of the areas not containing any fluorescence in the DAPI channel were identified using the same area selection from different places in the tile (Fig. 2.3), then mean (average) of the mean gray value was calculated to generate corrected total cell fluorescence (CTCF) values for each selected nucleus.

The Corrected Total Cell Fluorescence (CTCF) was calculated using this formula:

-   CTCF= IntDen – (Area x Background mean of the Mean Gray Value)

-   This formula was used to obtain CTCF of each selection area in the tile, then measurements were used to plot the values of Area in X axis with CTCF in Y axis as shown in results section and make graphs with Adobe Illustrator.

40

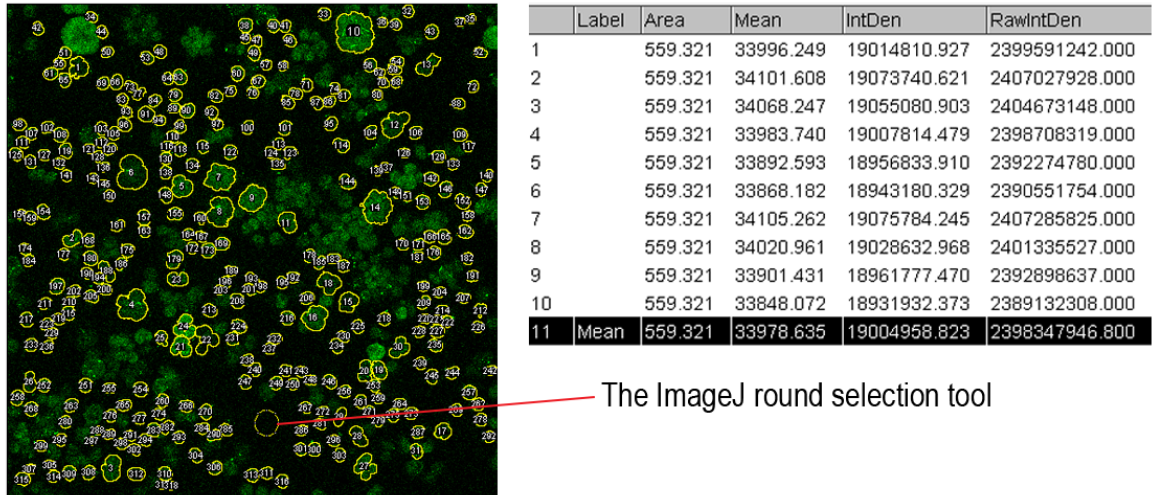|	Label	Area	Mean	IntDen	RawIntDen
1		559.321	33996.249	19014810.927	2399591242.000
2		559.321	34101.608	19073740.621	2407027928.000
3		559.321	34068.247	19055080.903	2404673148.000
4		559.321	33983.740	19007814.479	2398708319.000
5		559.321	33892.593	18956833.910	2392274780.000
6		559.321	33868.182	18943180.329	2390551754.000
7		559.321	34105.262	19075784.245	2407285825.000
8		559.321	34020.961	19028632.968	2401335527.000
9		559.321	33901.431	18961777.470	2392898637.000
10		559.321	33848.072	18931932.373	2389132308.000
11	Mean	559.321	33978.635	19004958.823	2398347946.800

The ImageJ round selection tool

Figure 2.3 Calculation of background fluorescence

10 different measurements were calculated from the tile background using the round selection tool. All selections have the same area. Descriptive data (Mean, Standard Deviation (SD), Min and Max) were also measured, but only the mean of the mean gray value of the10 measurements were used in the quantification.

2.2.8. β-Galactosidase In situ Assay for Cellular Senescence

10^6 cells (HEK293T or derivatives) were seeded in 6 well plates and incubated in tissue incubator until they were 70% confluent (over confluency was avoided because it can give false positive results). Adherent cells were washed with 1X PBS, then fixed in 4% Paraformaldehyde for 10 minutes at room temperature, then washed twice with 1X PBS. After that, cells were stained with freshly prepared staining solution in the dark overnight in a 37^0 C incubator (without CO_2). Cells were visualized and counted using an inverted Olympus IX70 microscope under 20x magnification objective, and images was acquired using a Kameram camera and software system.

3. RESULTS

3.1. Ccdc124 mutant HEK293T (H60 clone) Phenotype

A Ccdc124 mutant HEK293T (clone H60) was previously established in our laboratory in collaboration with Prof. Dr. Uygar Tazebay's laboratory at the Gebze Technical University Department of Molecular Biology and Genetics, using the CRISPR/Cas9 system[15,21]. Briefly, a CRISPR/Cas9 eukaryotic expression plasmid was generated targeting the third exon of the Ccdc124 gene, transfected into HEK293T cells and assessed by restriction fragment length polymorphism (RFLP) assays. Pools of mutant cells were single cell cloned and the area of interest surrounding the putative mutation site was amplified by the polymerase chain reaction from genomic DNA and sequenced by Sanger sequencing. Clone H60, which is extensively analyzed in this thesis, was identified to contain a 91 nucleotide deletion in one allele and a 24 nucleotide deletion in the second allele (as seen in Fig. 1.9 in the Introduction). In order to analyse the phenotype of these Ccdc124 mutant HEK293T (clone H60) cells, I performed confocal microscopy using a DAPI stain for nuclei contrasted with transmitted light captured by photomultiplier tube (T-PMT) that outlines cell shape. H60 cells contain two cell populations. The first population is normal-looking cells (NL) which are indistinguishable from non-mutant HEK293T in their shape. The second population consists of multinucleated cells (MN) which have an aberrant shape (Fig. 3.1A) in which they start to accumulate nuclei and become larger with continued culturing (Fig. 3.1B). Quantification of the two populations by image acquisition software demonstrated that MN cells were about 18% of the total population. The H60 clone has been continuously cultured in our laboratory for about 6 months and these two populations of cells co-exist as a stable cell phenotype.
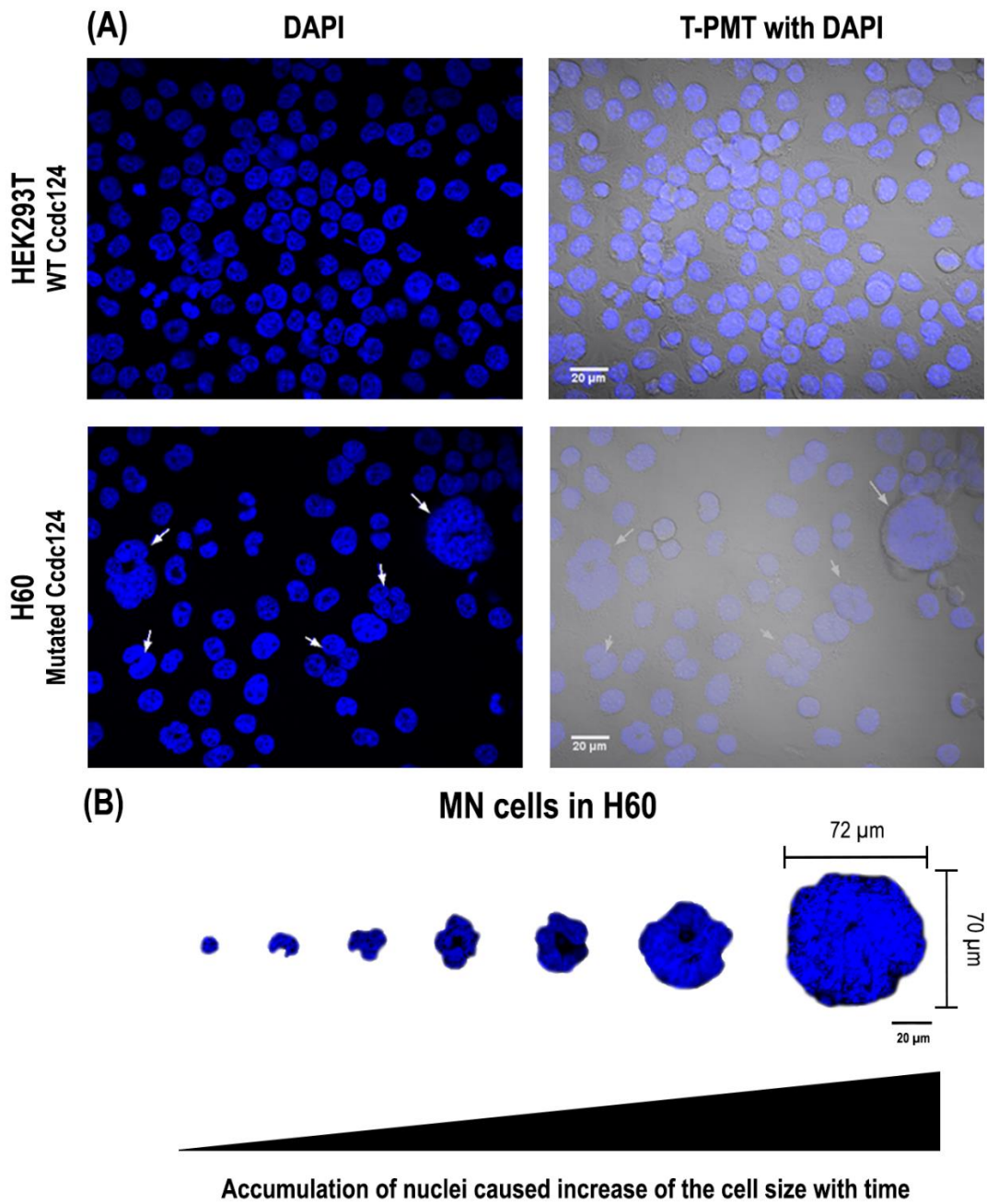
Figure 3.1 Phenotype of the Ccdc124 mutant HEK293T clone H60

(A) Ccdc124 mutated H60 cells have an aberrant multinucleated phenotype (MN), arrowheads point to these multinucleated cells. (B) MN cells increase in size with time due to accumulation of their nuclei, one cell nuclei size can reach up to 72 μm in diameter. DAPI was used for nuclei staining and the T-PMT channel was used to outline cellular shape. The scale bar is 20μm.

3.2. Cell Cycle Synchronization Analysis

3.2.1. Cell Cycle Synchronization Analysis using PI staining and FACS

To analyse the stages of mitosis and the subcellular localization of the Ccdc124 protein in HEK293T cells and the Ccdc124 mutated H60 clone with immunofluorescence and confocal microscopy, I synchronized the cell cycle. This process, which arrest all cells by thymidine and nocodazole treatment, releases all cells synchronously and is required to study the progression of cell cycle.

Firstly, I performed Propidium iodide (PI) staining and flow cytometry (FACS) analysis to observe and quantify the effects of the thymidine and nocodazole block on the cells. PI stains nuclear DNA and can be used to differentiate cells that have replicated their chromosomes in S from those in the G1 and G_2 phases. Thymidine blocks cells in the S phase by inhibiting DNA synthesis, and nocodazole blocks cells in the G_2/M phase because it inhibits microtubule polymerization. The PI staining procedure is outlined in the methods section 2.2.5.

In non-synchronized cells, most of the wild type HEK 293T cells were observed to be in the G1 phase (Fig 3.2 A) but when cells were blocked with thymidine (2mM) for 16 hours, the number of cells in S phase increased (Fig 3.2 B). In the case of the nocodazole block (50ng/μl) for 15 hours, the number of cells in the G2/M phase were significantly increased (Fig 3.2 C). The release of the HEK293T cells from this arrest with a further incubation in fresh medium for 90 minutes resulted in an increase in the percentage of cells in the G1 phase (Fig 3.2 D).
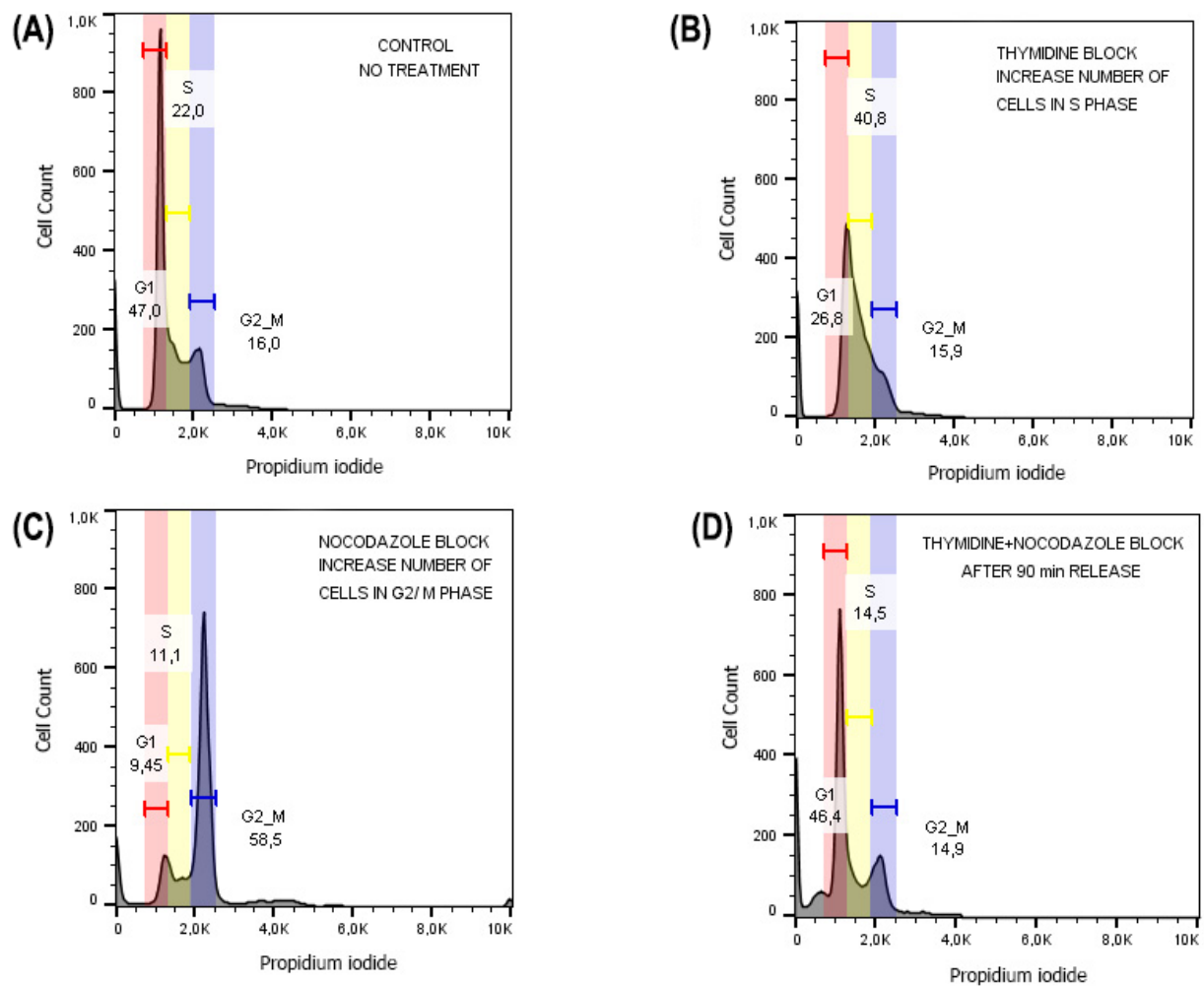
Figure 3.2 Wild Type HEK293T cell cycle synchronization analysis with PI staining and FACS

Non-synchronized cells are mainly in G1 phase. (B) After thymidine block for 16 hours, cells were blocked in phase. (C) After nocodazole block for 15 hours, cells were blocked in G_2/M phase. (D) After 90 minutes release, cell cycle returned to normal and increased in G1 phase.

3.2.2. Synchronized Cell Analysis using DAPI and T-PMT Microscopic Imaging

In order to visualize the synchronized cells and identify the time required to synchronize cells in each mitotic stage, I performed a double thymidine block with nocodazole (cell cycle synchronization procedure explained in the methods section 2.2.3). Cells were released with fresh medium and incubated for 0, 15, 30, 45, 60 or 90 minutes and fixed by paraformaldehyde treatment. DAPI was used to stain nuclei.

At 0 minutes (immediately after nocodazole treatment) most cells were observed to be in prophase in which chromatin condensation takes place to form visible chromosomes. After 15 minutes, most of the cells were in metaphase, where chromosomes started to align in the middle of the cell. After 30 and 45 minutes, cells were in early and late anaphase in which chromosomes started to separate from each other towards opposite pole of the cells. After 60 minutes, cells were at telophase in which the cleavage furrow started to separate cytoplasm of the two daughter cells. After 90 minutes most cells finished mitosis and they returned to interphase (Fig.3.3).
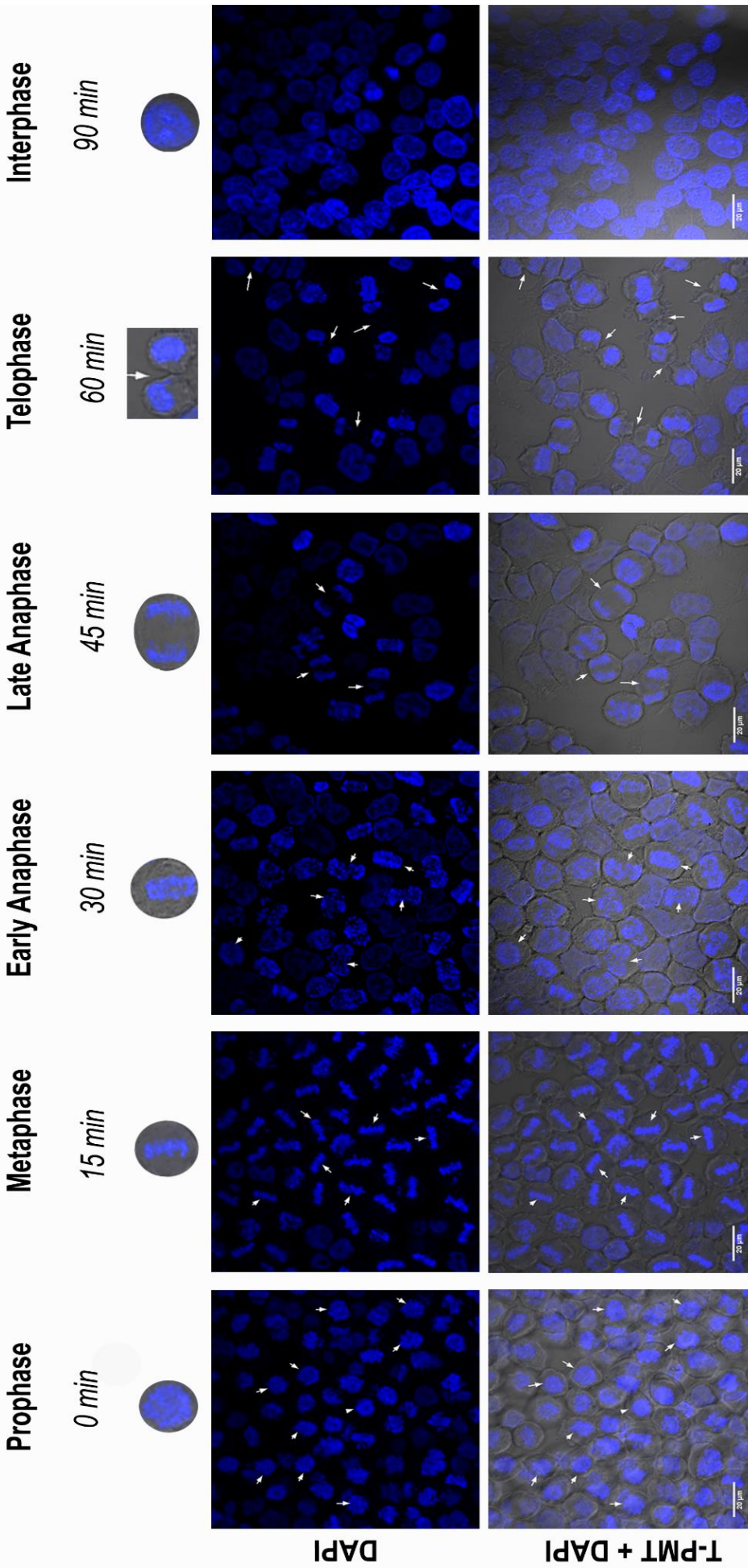
Figure 3.3 Synchronized WT HEK293T mitotic stages

After release of cells from growth arrest, mitotic stages were seen in these time intervals; in Prophase at 0 minute. Metaphase at 15 minutes. Early and late Anaphase at 30 and 45 minutes respectively. Telophase at 60 minutes. After 90 minutes most cells finished mitosis and returned back to interphase. DAPI was used to stain nuclei and T-PMT was used to see the cells. Scale bars equal 20μm.

3.3. Subcellular Localization of Ccdc124 During Mitosis

3.3.1. Interphase

In order to find the subcellular localization of the Ccdc124 protein in WT HEK293T and the mutant clone H60 during mitosis and analyze mitosis stages, I performed immunofluorescence using an anti-mid-Ccdc124 antibody recognizing the central part of the protein (between residues 100–150) and an anti-gamma tubulin antibody as a centrosome marker (samples preparation is described in the methods section 2.2.4.1.). After imaging of non-synchronized cells, I observed focal staining in WT HEK293T and in normal-looking (NL) H60 mutant cells, mostly near the nuclei when cells are in interphase. In contrast, in the MN, bigger structures, this focus was mostly in the center of the cells. This can indicate a clustering of centrosomes, due to the failure of cytokinesis. Such accumulation of centrosomes has previously been observed in the literature and is termed centrosome amplification or supernumerary centrosomes. In WT HEK293T, NL and MN cells, Ccdc124 colocalized with gamma tubulin (Fig. 3.4).

3.3.1. Prophase

The prophase stage of the cell cycle is characterized by starting chromatin condensation and the replication of the centrosomes. Gamma-tubulin colocalized with Ccdc124 at two dot-like structures in WT HEK293T and NL cells. Two dots was observed as a result of the replication of the centrosome at this stage. In comparison, multiple bigger structures represented the centrosomes were observed and colocalization was not obvious in the MN cells (Fig.3.5).

Interphase
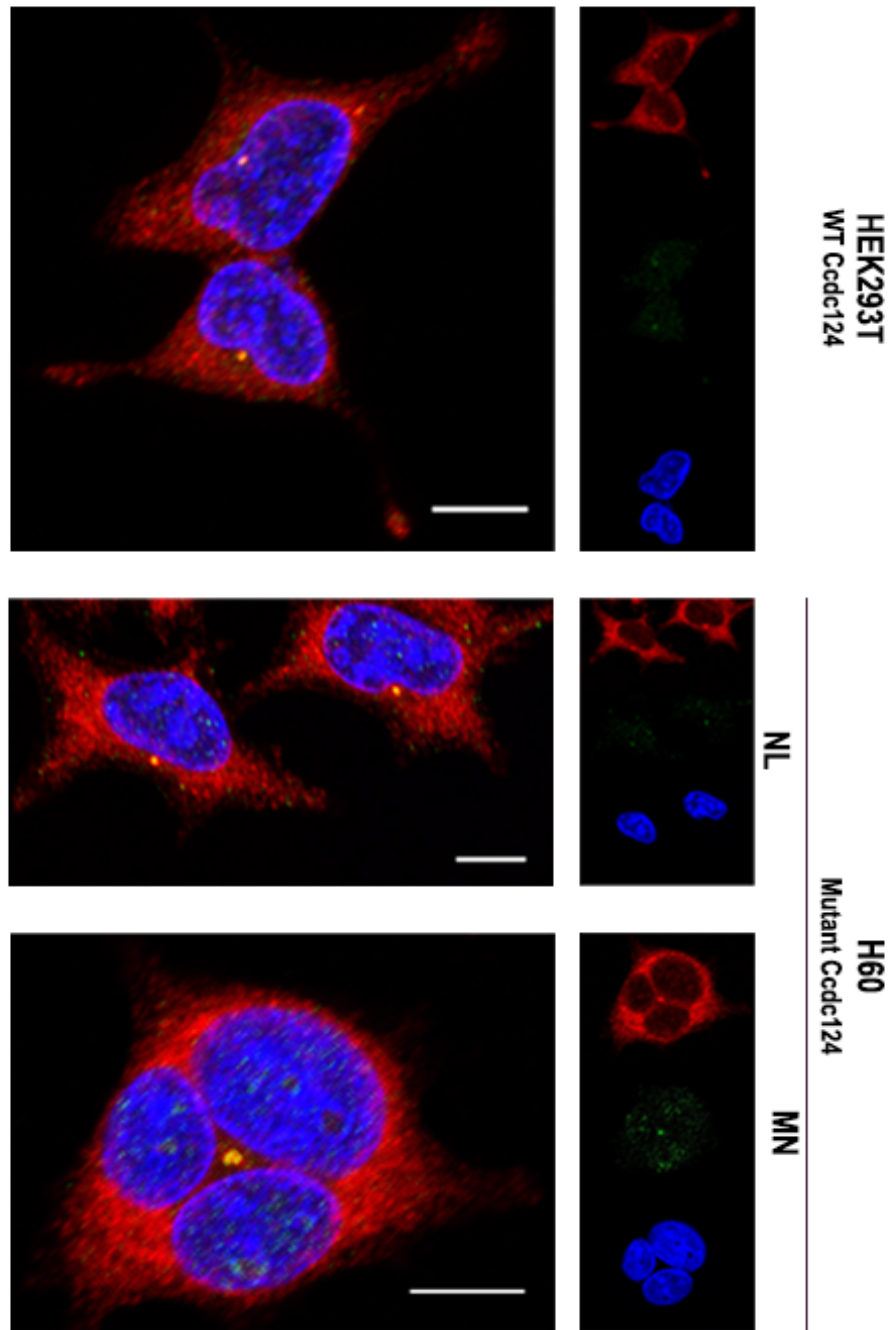
Red channel: Anti-gamma tubulin - Centrosome marker
Green channel: Anti-Ccdc124
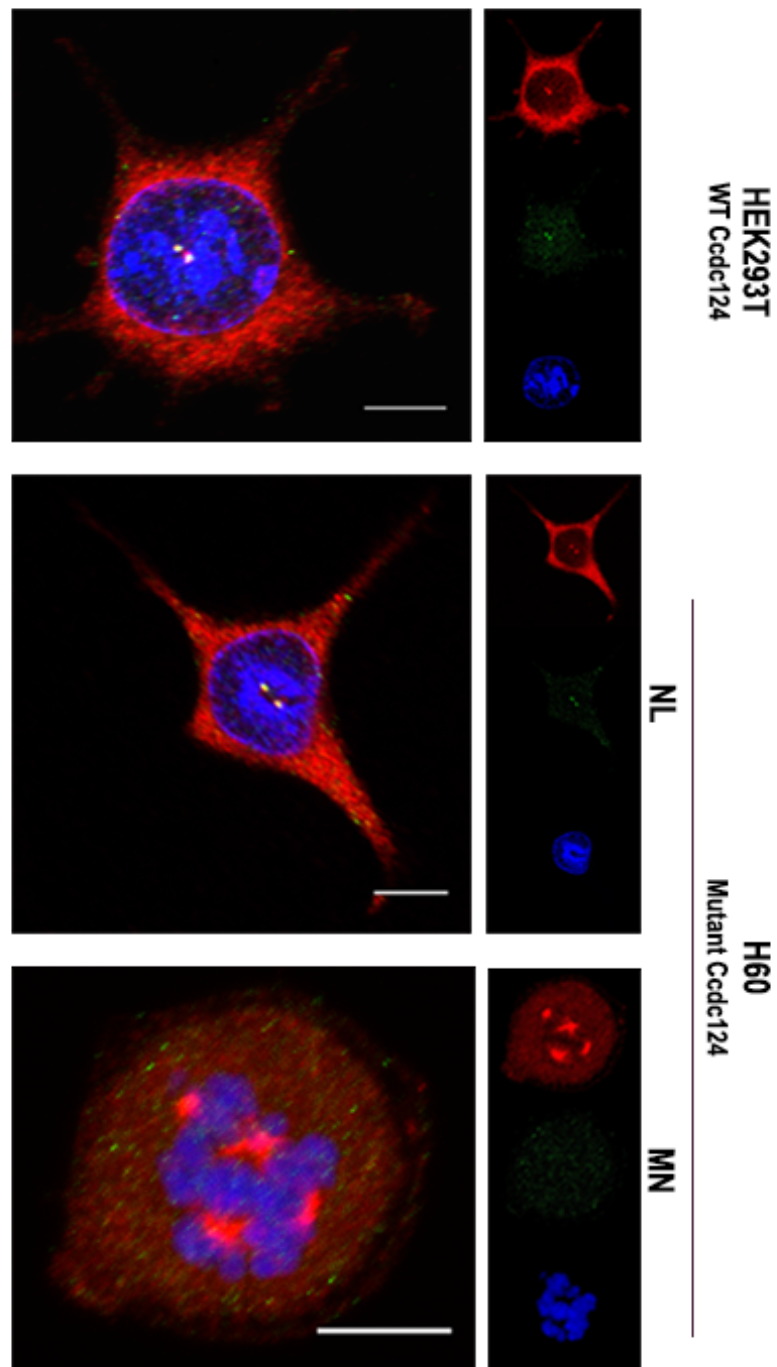Blue channel: DAPI to stain DNA
10µm scale bar

Figure 3.4 HEK293T and H60 mutant cells in Interphase

Gamma-tubulin colocalized with Ccdc124 protein in both WT and mutated HEK293T cells. In WT and NL cells a dot-like structure was observed, while a bigger structure in the center of the cell was observed in the MN cells this may be a result of centrosome clustering after cytokinesis failure.

49

Prophase

Red channel: Anti-gamma tubulin - Centrosome marker
Green channel: Anti-Ccdc124
Blue channel: DAPI to stain DNA
10μm scale bar

Figure 3.5 HEK293T and H60 mutant cells in Prophase

In prophase, chromatin condensation started and two dot-like structures was observed in both WT HEK293T and NL cells due to replication of centrosome at this stage and gamma tubulin colocalized with Ccdc124, while in the MN cells colocalization was not seen. Formation of multiple centrosomes was observed in the MN cells.
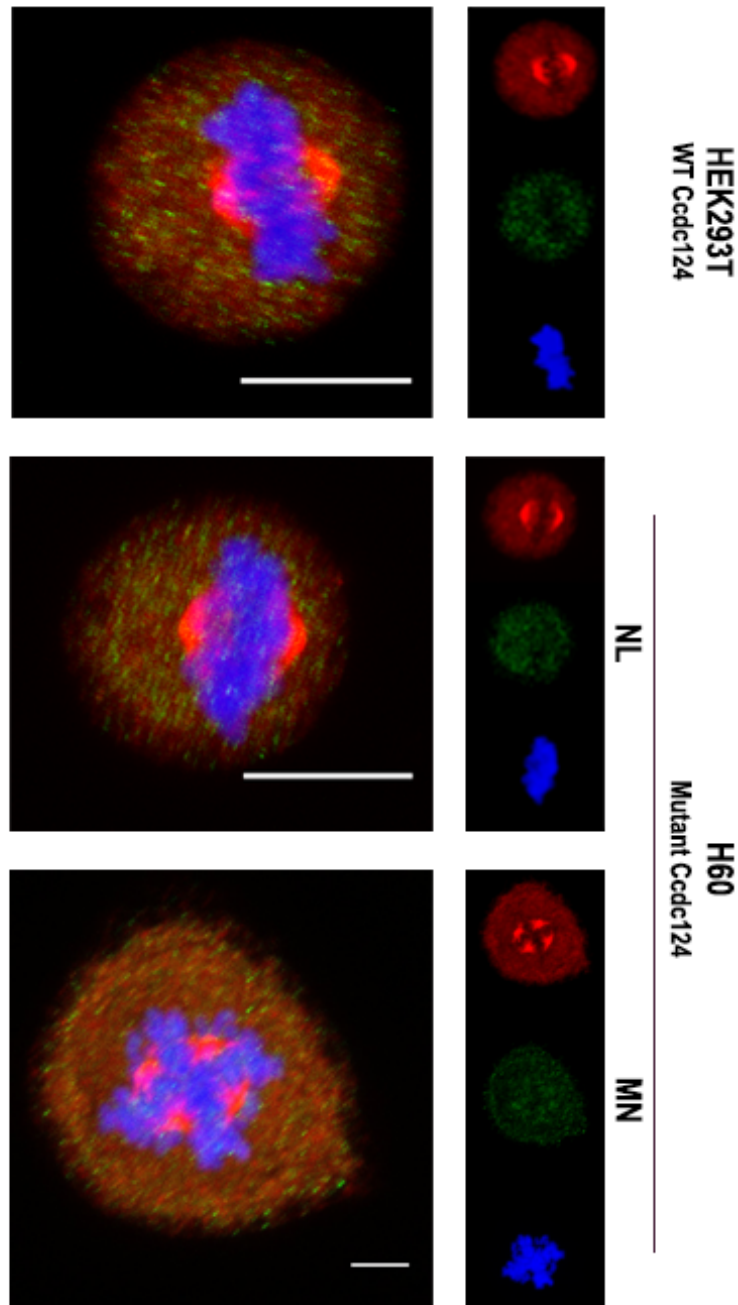
3.3.2. Metaphase

In metaphase, chromosomes were aligned at the equator of the cell and diploid mitotic spindles were formed in both WT HEK293T and NL cells. The mitotic spindle pole is generally formed by one centrosome composing of a pair of centrioles embedded in pericentriolar material (PCM) that contains the γ-tubulin ring complexes (γ-TuRCs) from which microtubule nucleation is initiated[22]. The presence of two centrosomes forms diploid mitotic spindles that is crucial for the bi-orientation and precise segregation of chromosomes to two daughter cells. Diploid spindles lead to proper chromosome alignment at the equator of the cell, and ensure faithful segregation of chromosomes at anaphase, however multipolar spindles were formed in the MN aneuploid cells which caused misalignment of chromosomes in different directions (multipolar metaphases) in the cell. Mitotic spindle multipolarity happens due to different aberrations, such as de novo centriole assembly, centriole overduplication, mitotic slippage, cytokinesis failure, and cell fusion. In the MN cells, presence of multiple centrosomes caused multipolar spindle formation. Aneuploidy was identified to be associated with formation of multipolar spindles and supernumerary centrosomes. No colocalization of Ccdc124 with gamma-tubulin was observed in the three cell types at this stage (Fig.3.6).

3.3.1. Anaphase

During anaphase, chromosomes where properly segregated to each opposite pole of the cell due to formation of diploid mitotic spindles in WT HEK293T and NL cells, but chromosomes were missegregated to different sides in the MN cells because they have multiple centrosomes and each one form mitotic spindle. When the cell has multipolar spindles they cause the misalignment and missegregation of chromosomes that I observed in the MN cells. Mitotic spindle multipolarity has been used for diagnosis of the pathologic mitosis in human tumours. The formation of multipolar spindles is usually accompanied with supernumerary centrosomes and chromosomal instability[22]. The chromosomes instability and chromosome attachment errors are more explained in section 3.4. Colocalization of Ccdc124 with gamma-tubulin is observed in all three cell types (Fig.3.7).

Metaphase

Red channel: Anti-gamma tubulin - Centrosome marker
Green channel: Anti-Ccdc124
Blue channel: DAPI to stain DNA
10µm scale bar

Figure 3.6 HEK293T and H60 mutant cells in Metaphase

Normal diploid mitotic spindles were formed in both WT HEK293T and NL cells which lead to correct chromosome alignment at center of the cell but in the MN cells, multipolar spindles were formed as a result of presence of multiple centrosomes which cause misalignment of chromosomes in different directions.
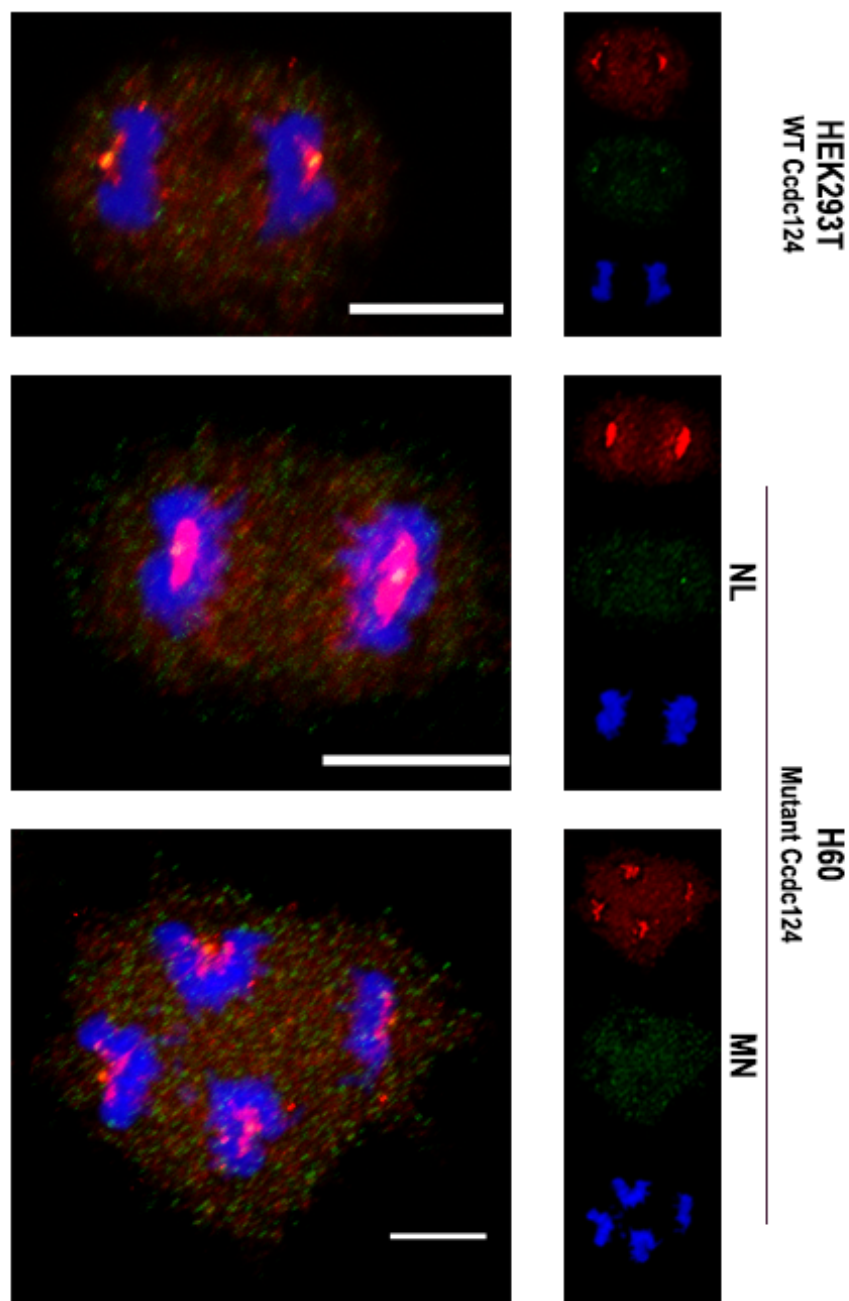
Anaphase

Red channel: Anti-gamma tubulin - Centrosome marker
Green channel: Anti-Ccdc124
Blue channel: DAPI to stain DNA
10µm scale bar

Figure 3.7 HEK293T and H60 mutant cells in Anaphase

Chromosomes were properly segregated due to formation of dipolar spindles in the WT HEK293T and NL cells, but the multipolar spindles in the MN cells caused missegregation of chromosomes.

53

3.3.2. Telophase

The WT HEK293T and NL cells had normal telophase in which the chromosomes decondense as the nuclear envelopes reform around the two daughter nuclei and the cleavage furrow was formed to separate cytoplasm of the two daughter cells. Cells in telophase can be observed in figure 3.8, where WT and NL Ccdc124 mutant cells have ingression furrows that start to separate the two daughter cells. Such structures were not observed on MN Ccdc124 mutant cells.

3.3.3. Cytokinesis

At the end of telophase the midbody is formed at the midzone of the intercellular bridge to mark the site of abscission. At this stage the Ccdc124 protein is recruited to midbody region after dissociation from the centrosome, but what trigger this relocation is not known yet. The MN cells fail to separate their cytoplasm (Fig.3.9). The lack of telophase and cytokinesis in MN cells results in the formation of aneuploid cells.

Telophase
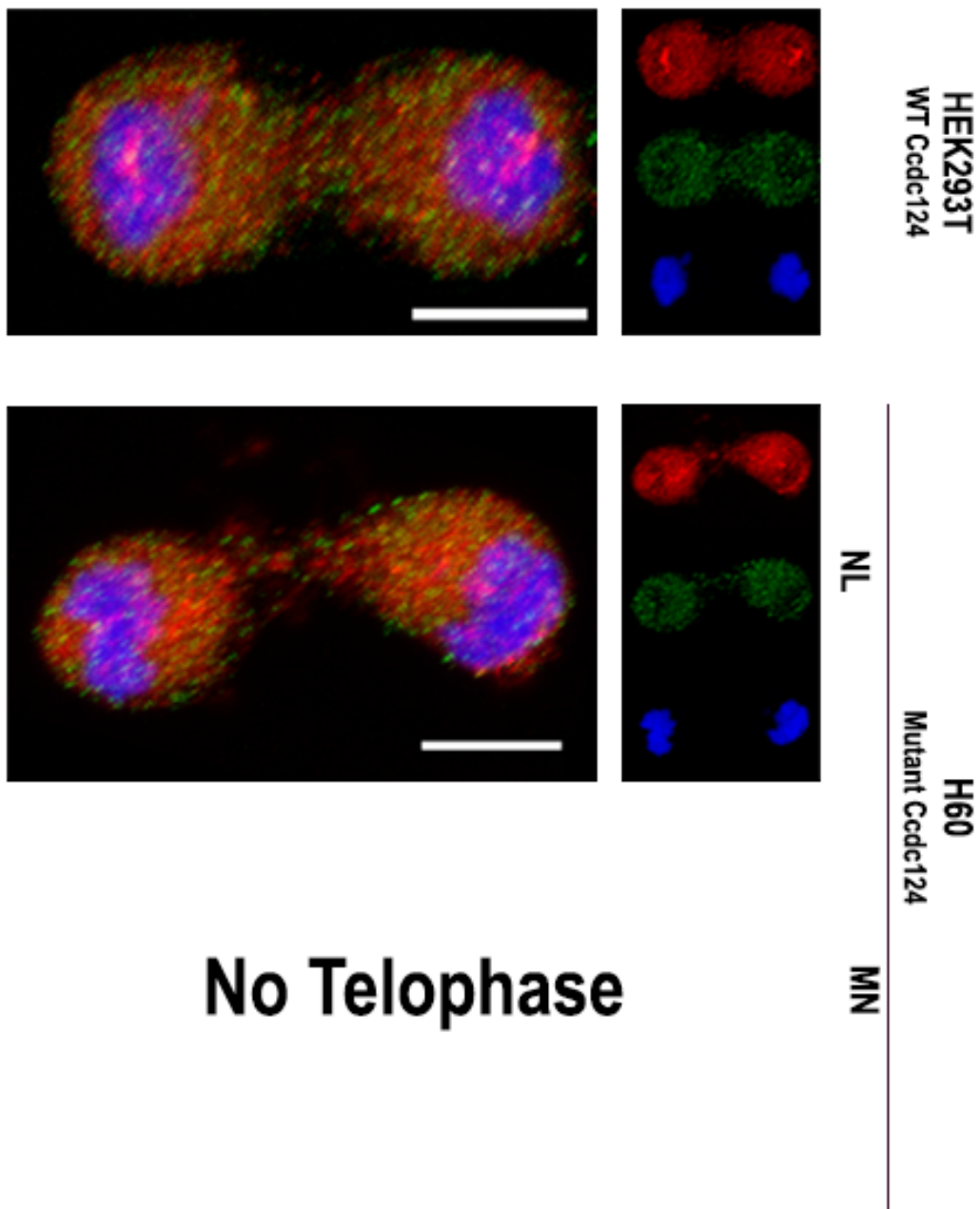
Red channel: Anti-gamma tubulin - Centrosome marker
Green channel: Anti-Ccdc124
Blue channel: DAPI to stain DNA
10μm scale bar

Figure 3.8 HEK293T and H60 mutant cells in Telophase

At telopase cleavage furrow starts to form between the two daughter cells which is followed by cytokinesis and abscission process.
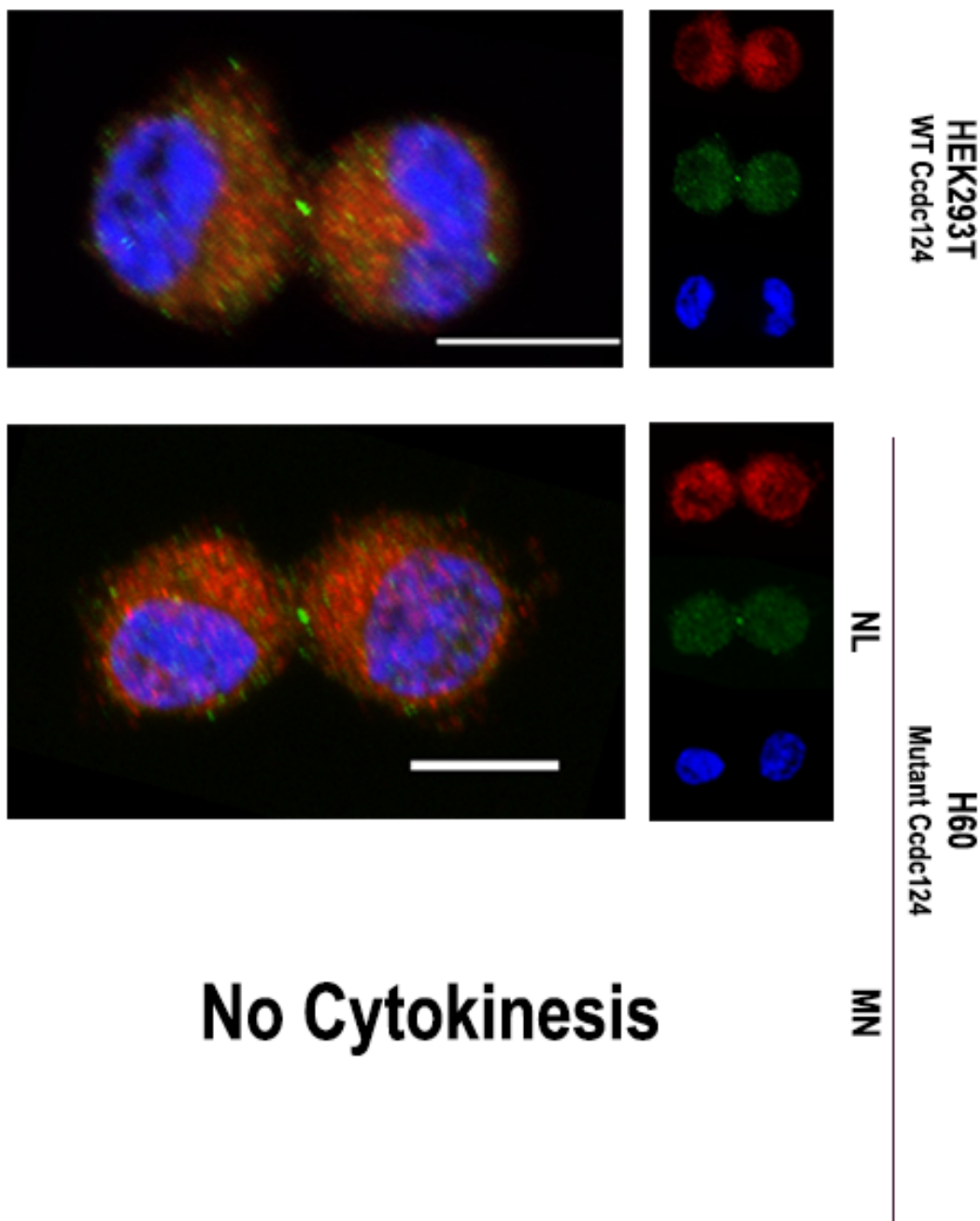
Figure 3.9 HEK293T and H60 mutant cells during Cytokinesis

At cytokinesis, midbody is formed to complete abscission process, at this stage the Ccdc124 protein is recruited to the midbody. Arrowhead points to the Ccdc124 protein at the midbody.

3.4. Chromosome and Mitotic Aberrations in the MN Cells

Similar to DNA, centrosomes typically replicate only one time at each cell cycle. Thus, in mitosis, two centrosomes insure the formation of bipolar mitotic spindle which is important for the bi-orientation and correct segregation of chromosomes to be evenly distributed between the two daughter cells. Chromosomes must develop accurate 'amphitelic' attachments with the mitotic spindle microtubules, in which a single kinetochore attaches to microtubules arising from one of the mitotic spindle poles and the sister kinetochore attaches to the microtubules arising from the opposite spindle pole[22]. The knock out or mutation of the Ccdc124 gene caused cytokinesis failure in the MN cells which led to mitotic aberrations such as centrosome amplification (multiple or supernumerary centrosomes), multipolar spindle formation, and chromosome attachments errors such as monotelic or merotelic chromosomes. Monotelic chromosomes arise when only one sister kinetochore in a pair of sister kinetochores is attached to kinetochore microtubules. Merotelic chromosomes arise when incorrect microtubule–kinetochore attachment happens in which a kinetochore becomes attached to microtubules from both spindle poles. It was demonstrated before that the aneuploid tumour cells have similar mitotic errors and the centrosome amplification is an important cause of chromosome attachment errors[23].

In WT HEK293T and NL cells bipolar spindles were formed and I did not observe any chromosomes attachment aberrations. In contrast, the MN cells had multiple centrosomes that caused multipolar spindles formation and subsequent monotelic or merotelic chromosome attachments. Most of the merotelically attached chromosomes segregate correctly during anaphase, however, some of them remain firmly attached to both spindle poles and cannot move towards the poles in anaphase. The unresolved merotelic attachments chromosomes in anaphase can cause lagging chromosomes (a single chromosome that lag between two masses of segregating chromosomes during anaphase) (Fig.3.10 and 3.11). Lagging chromosomes can either be missegregated, which leads to formation of two aneuploid daughter nuclei or the lagging chromosomes that cannot reach

the separated chromosome masses adjacent to the opposite poles and fails to be included to the daughter nucleus can reassemble a nuclear envelope and forms a micronucleus (Fig.3.12 and 3.13). The chromosomes that are incorporated in micronuclei have an increased number of DNA breaks in the following cell cycle because of the abnormal DNA replication or the cell undergo mitosis while the micronuclei is still replicating their DNA[23]. Micronuclei formation is a biomarker of genotoxic events and chromosomal instability. These nuclear aberrations are usually observed in tumour cells which indicates presence of damaging events in the genome that possibly increase risk rate of developmental and degenerative diseases. In addition, origination of micronuclei can occurs due to chromatid fragmentation that is caused by misrepair or unrepaired DNA breaks. Missegregation of whole chromosomes during anaphase can also cause micronuclei formation as a consequence of hypomethylation of repeat sequences in centromeric and pericentromeric DNA, abnormalities in kinetochore proteins or their organization, defective spindle and anaphase checkpoint genes[24].

In addition, I observed centrosome clustering during mitosis in the MN cells (Fig.3.14). Centrosome clustering happens when two centrosomes approach from each other and form a single spindle pole. This mechanism was identified in tumour cells that have supernumerary centrosomes and centrosome clustering help them to avoid the lethal multipolar divisions[25].

These errors cause chromosome instability (CIN) which is a condition that is characterized by high rates of chromosome gain and loss during divisions. This was observed in the MN cells in the formation of unequal nuclei sizes, which may be caused also by nuclei fusion. I made a model for the mechanism of the MN cells formation, and represent the mitotic aberrations of supernumerary centrosome and multipolar spindles formation and chromosome attachment errors that I observed in the MN cells (Fig.3.10).

Cytokinesis failure

Binucleated cell with two centrosomes

Ccdc124 -/-

Merotelic chromosome when a single kinetochore simultaneously connects to both spindle poles

Monotelic chromosome is only attached to one spindle pole

Lagging chromosome is single chromosomes that lag between the two masses of segregating chromosomes during anaphase

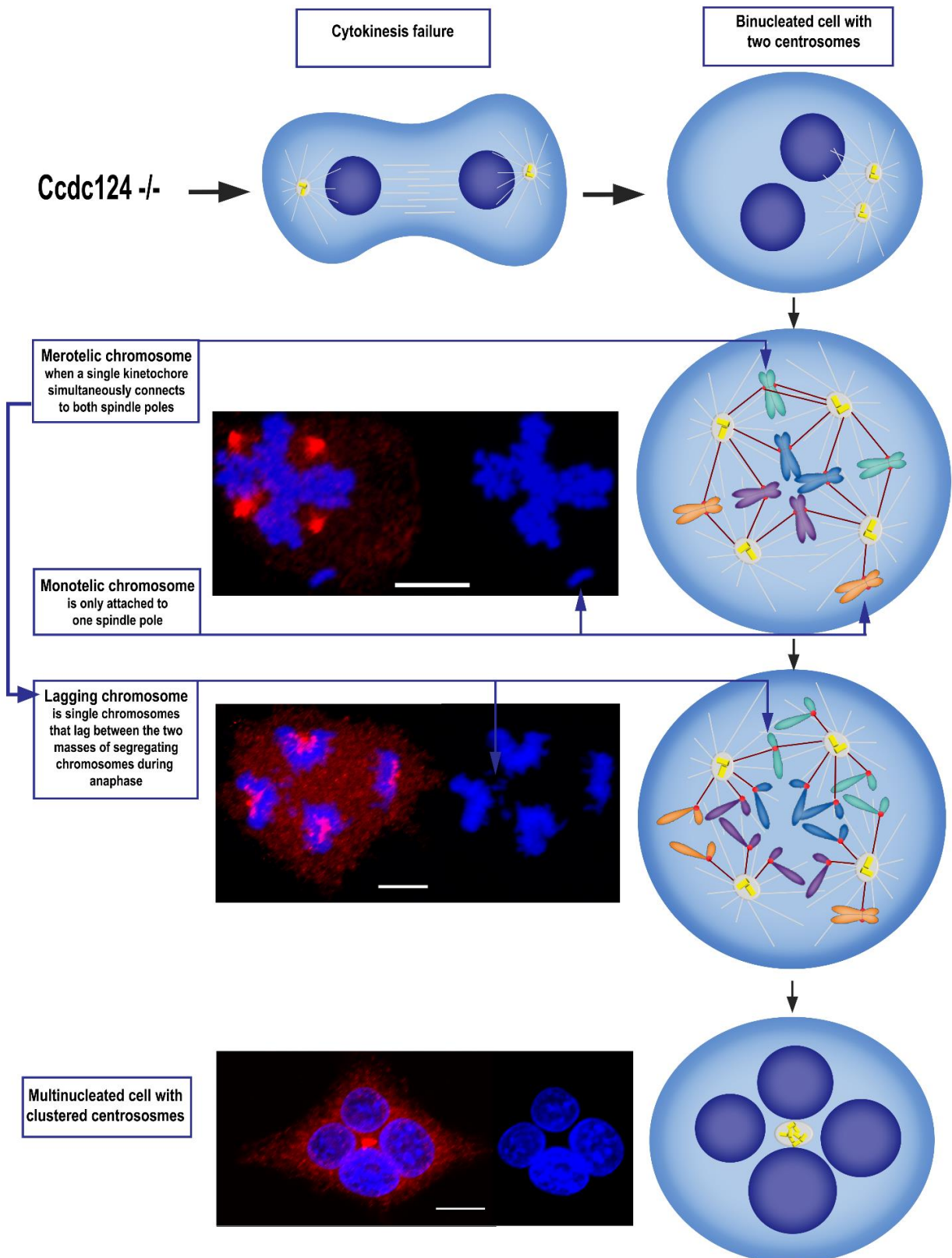**Multinucleated cell with clustered centrososmes**

Figure 3.10 Chromosome and mitotic aberrations in MN cells

In this model, a binucleated cell is formed after cytokinesis failure. Cells can enter subsequent endoreduplication of nuclei without cytoplasmic division, the supernumerary centrosomes in the cell formed multipolar spindles that lead to the subsequent misalignment and segregation of chromosomes. Some errors in chromosome attachments were observed such as monotelic attachment in which the chromosome is only attached to only one mitotic spindle and merotelic attachment in which a single kinetochore is attached to two mitotic spindles which can lead to the formation of a lagging chromosome in anaphase. Subsequent formation of a nuclear membrane around each daughter nuclei, also clustering of centrosomes at the center of the cell between the nuclei can be seen. The scale bar is equal to 10μm.
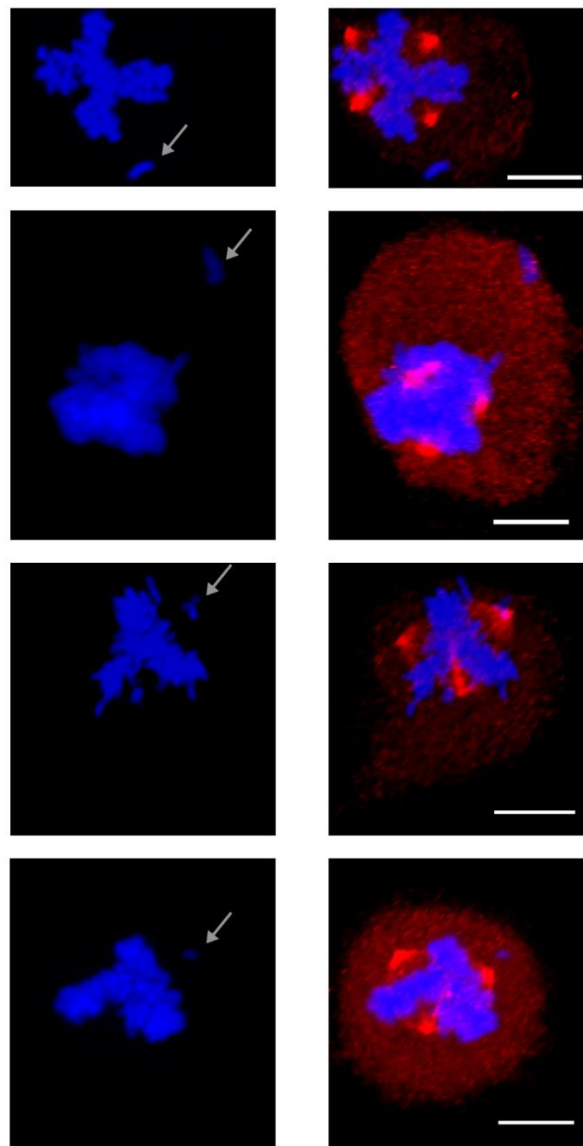

Figure 3.11 Chromosomes attachment errors in MN cells

MN cells were synchronized with double thymidine block followed by nocodazole treatment then stained with anti-gamma tubulin (red) and DAPI for nuclei (blue). Properly unaligned chromosomes were observed in several MN cells during anaphase or metaphase.
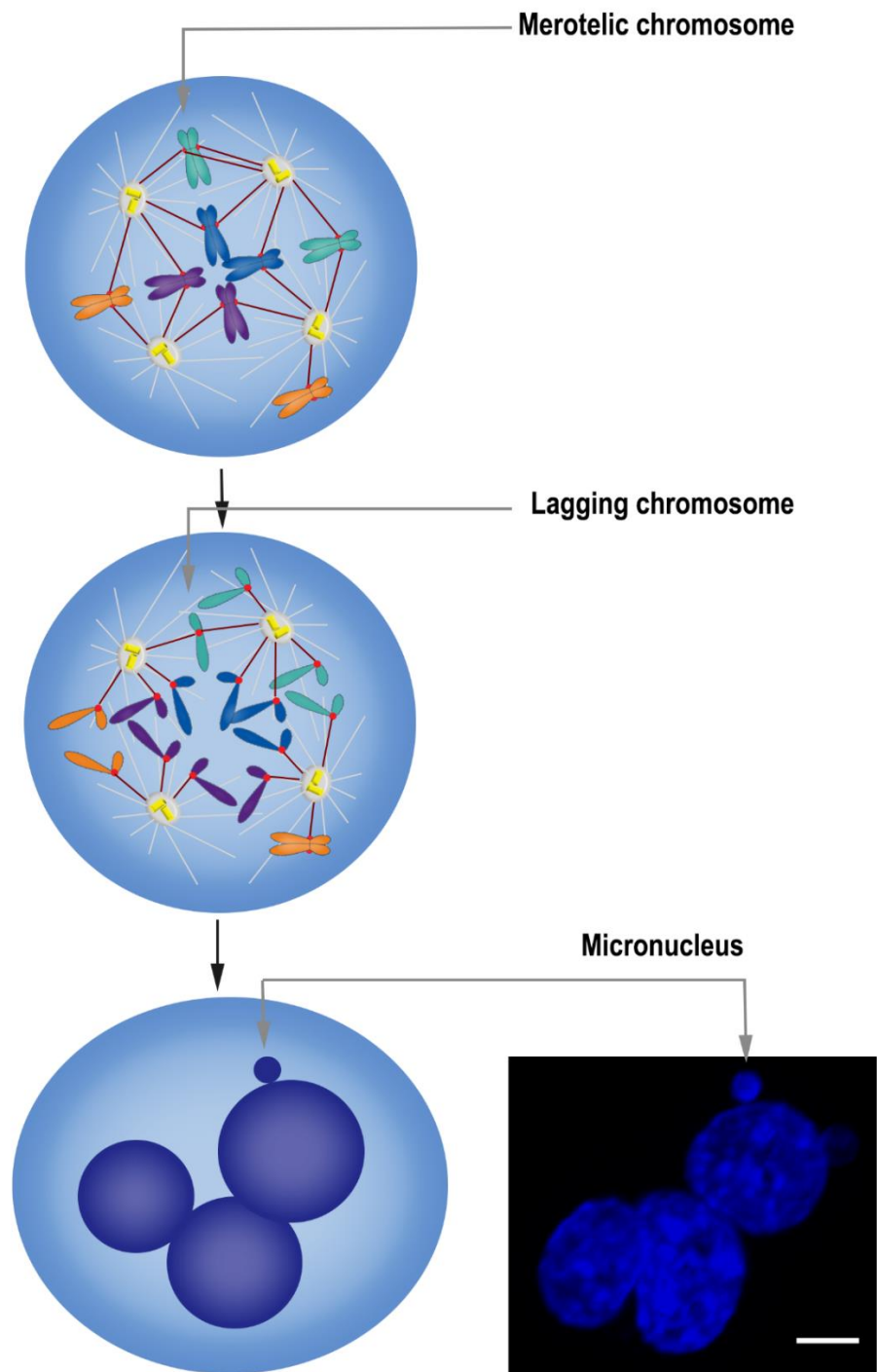
Figure 3.12 Chromosome missegregation results in the formation of a micronucleus in MN cells

The unresolved merotelic attachment in metaphase forms a lagging chromosome in anaphase. The lagging chromosome that was missegregated and failed to incorporate into the daughter nucleus formed a micronucleus. In lower right picture the nuclei were stained with DAPI.
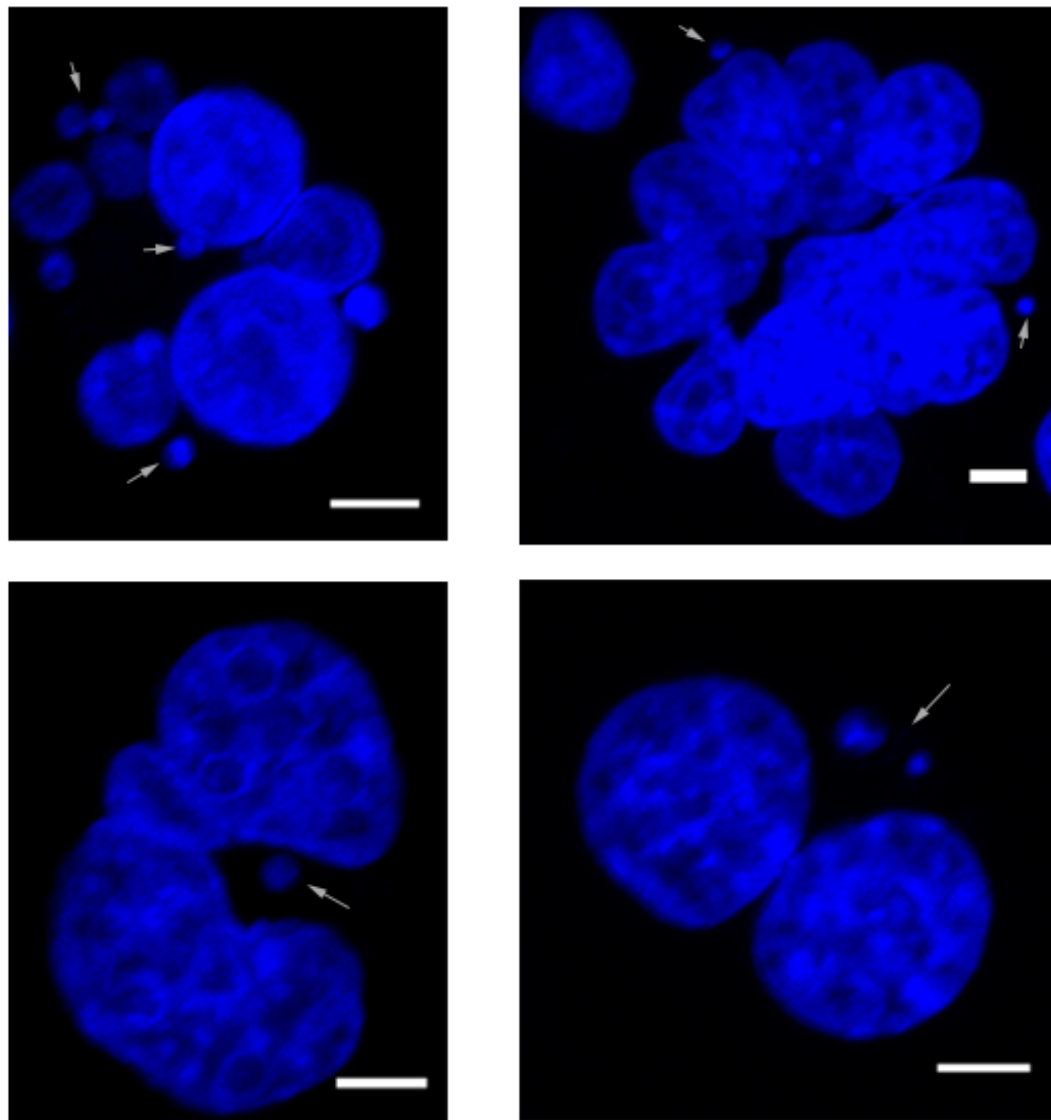
Figure 3.13 Micronuclei in the MN cells

Micronuclei formation in the MN cells were an obvious feature that was observed in multiple MN cells. Nuclei were stained with DAPI. The scale bars equal 5μm.
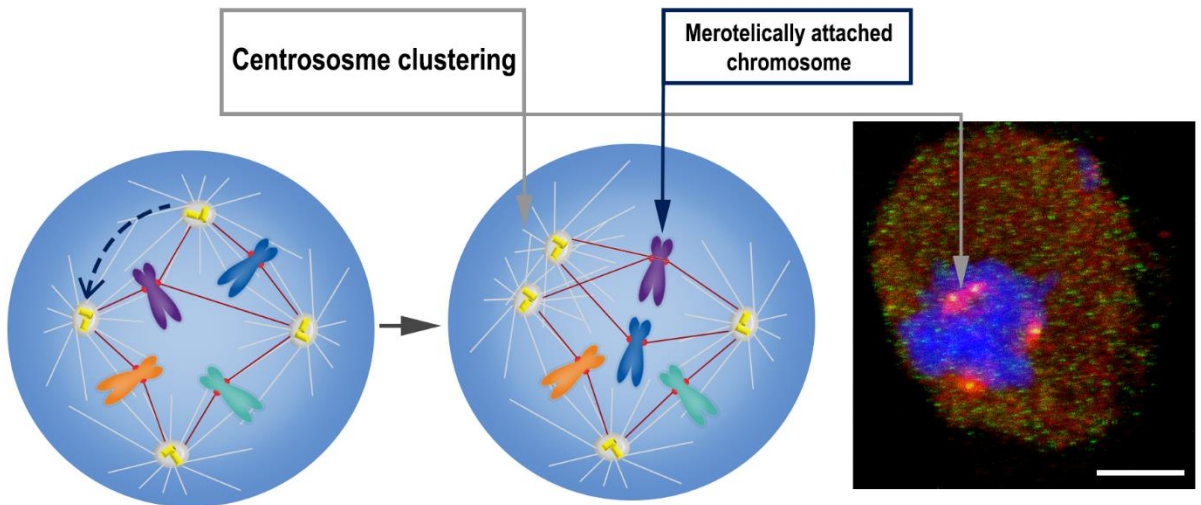
Figure 3.14 Centrosome clustering in the MN cells

The MN cells have multiple centrosomes. It has been reported that aberrant cytokinesis can results in centrosome clustering before anaphase. Centrosome clustering increase the frequency of merotelic attachments in which a single kinetochore attaches to microtubules arising from both sides of the spindle. The image on the right is a MN cell in prometaphase, centrosome clustering can be seen as two big red dots that represent the gamma tubulin and the two smaller green dots represent the Ccdc124 centrosomal protein. The two centrosomes clustered to form a single spindle pole. DAPI used for nuclei. Scale bar equals 10μm.

3.5. Upregulation of p53 in The Multinucleated Cells (MN)

3.5.1. Analysis of p53 Upregulation Using Immunofluorescence

Aneuploidy was associated with cell cycle arrest and the tetraploid cells generated by experimentally induced mitotic failure undergo a p53- dependent arrest[26–28]. P53 is an important stress responsive tumour suppressor protein that has roles in cell cycle arrest, senescence, apoptosis, autophagy and DNA repair. In normal conditions, p53 levels are very low in the cell. The mechanism that keeps p53 levels low is mediated by p53 binding proteins that cause p53 ubiquitination and degradation. Mouse double minute 2 (MDM2) is a p53 E3 ubiquitin ligase that binds to p53 and promotes its ubiquitination and degradation[29]. Stress inducing conditions such as DNA damage cause p53 phosphorylation, dissociation from MDM2, stabilization and activation that leads to accumulation of p53 in the cell. The activated p53 translocates to the nucleus to bind to its target genes.

Cytokinesis failure and aneuploidy were identified to result in activation and upregulation of p53[30,31]. Therefore, I wanted to check if p53 protein is upregulated in the MN cells, which clearly have a stressed phenotype. I performed an immunofluorescent staining using anti-p53 monoclonal mouse antibody (description of the immunofluorescence procedure is shown in the methods section 2.2.4.2) and after image acquisition I observed an increase in the p53 fluorescence in the MN cells compared to the NL or WT HEK293T cells (Fig.3.15). I used the WT HEK293T cells as a positive control for this experiment. I treated the cells with the anticancer drug, Cisplatin (100 mM for 24 hours) that causes DNA damage and upregulation of the p53 protein. The activated p53 accumulated and translocated to the nuclei (Fig. 3.15). A second positive control was HCT116 cells (colon cancer cell line), that were treated with the anticancer drug, Doxorubicin (1µM for 8 hours), that induces DNA damage and upregulation of p53. Without Doxorubicin treatment, HCT116 cells have low levels of p53 in the cytoplasm, but the treated cells had a very clear

increase in p53 levels in both cytoplasm and nucleus (Fig. 3.16). To prove that the upregulation of p53 protein levels was in the MN cell population, I quantified of p53 levels using ImageJ software that is explained in the following section.
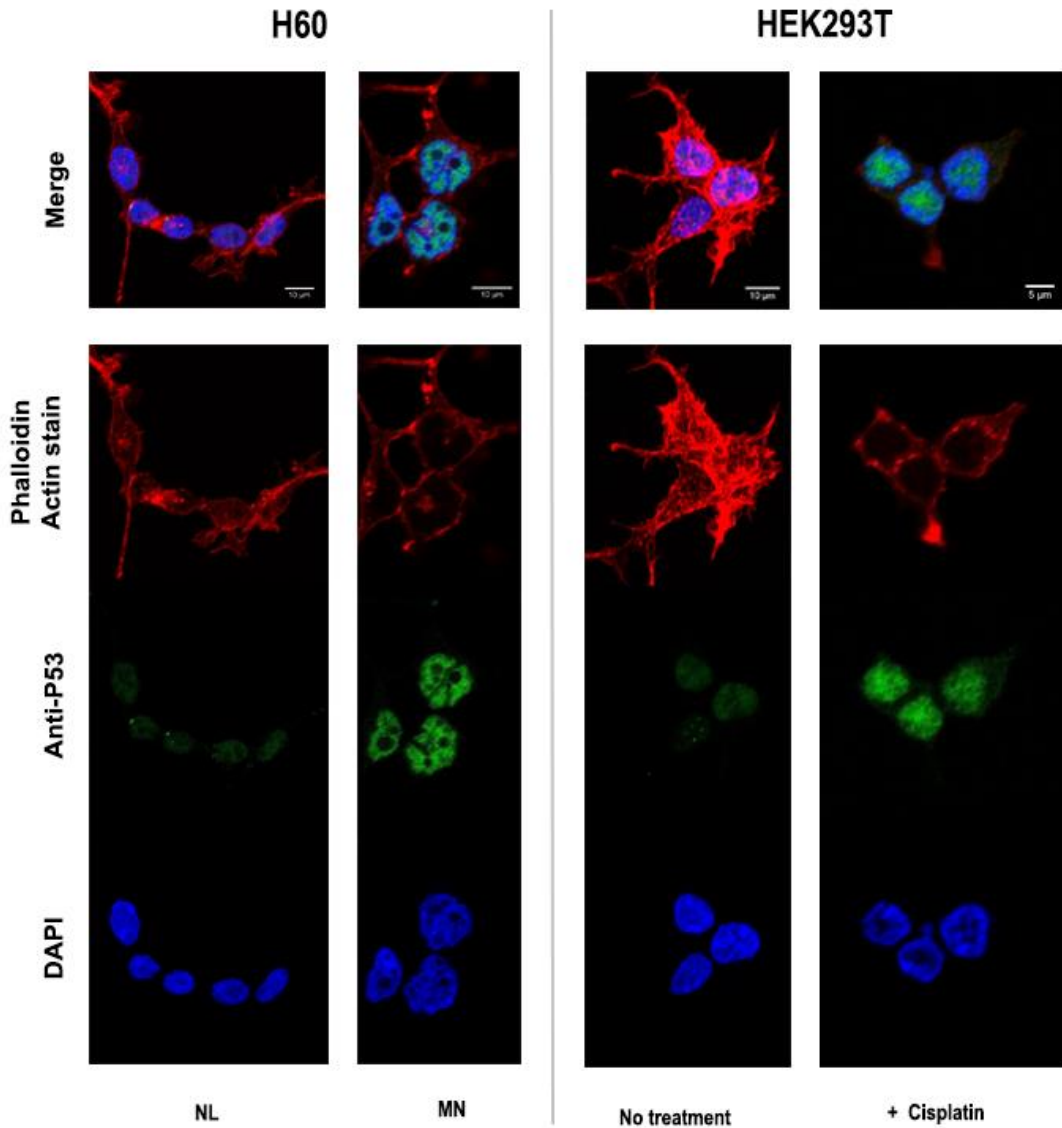
Figure 3.15 P53 upregulation in the MN cells

P53 fluorescence levels are increased in the MN cells compared to WT HEK293T or NL cells. Increase of p53 levels is an indication that the MN cells area under stress. Appositive control for this experiment was the WT HEK293T cells which were treated with 100 μM of Cisplatin for 24 hours. A clear increase of p53 levels in the treated cells after DNA damage. Anti-p53 mouse monoclonal antibody was use to stain p53 protein. Phalloidin was used to stain actin filament to show cells outline and DAPI for nuclei.
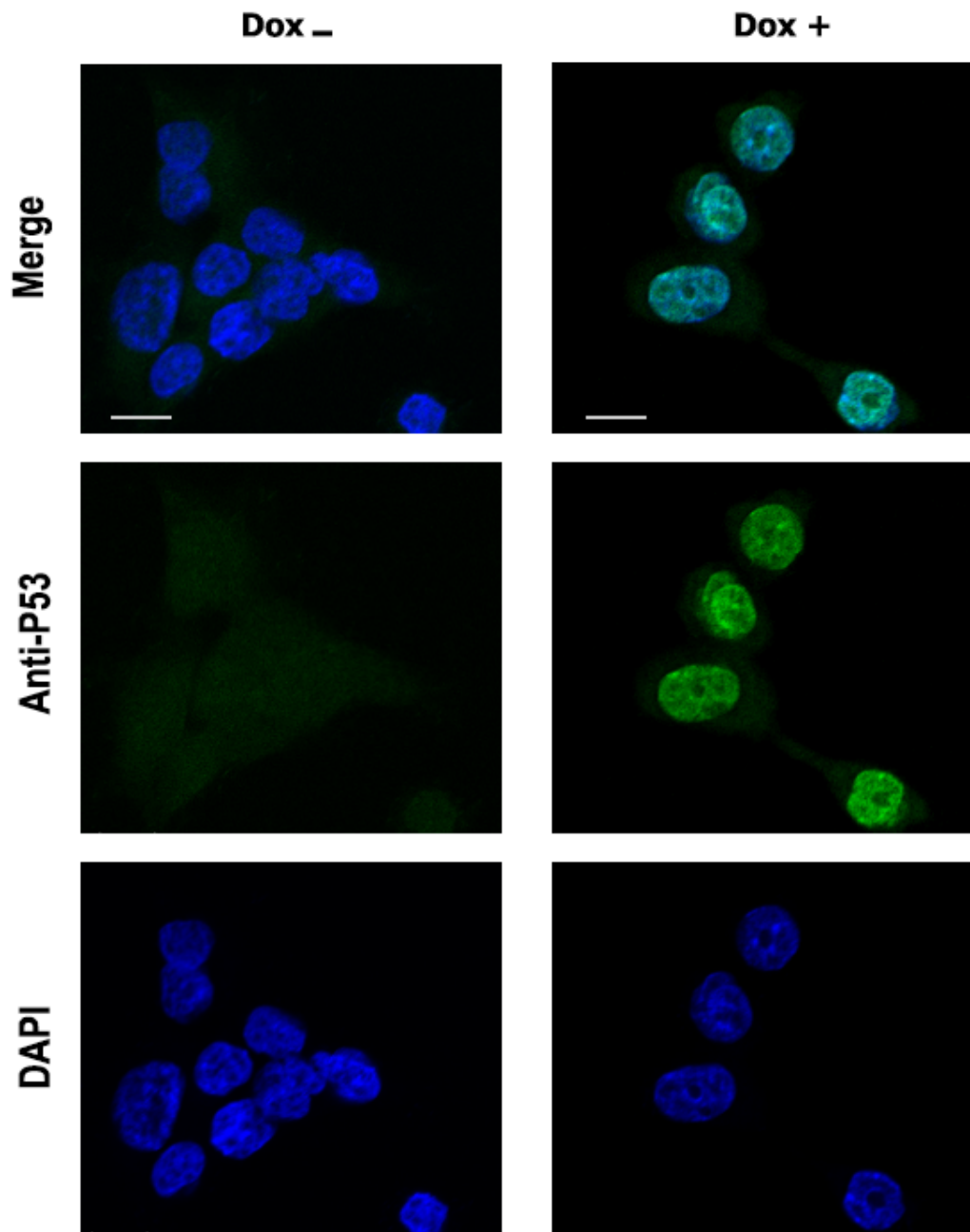
Figure 3.16 P53 upregulation in HCT116 cells as a positive control

The HCT116 cells were used as a positive control of p53 levels upregulation. Cells were treated with with the anticancer and DNA damaging drug Doxorubicin (1µM for 8 hours). Cells without treatement have very low amount of p53 in the cytoplasm. In contrast the treated cells had very clear increase in p53 fluorescence both cytoplasm and nuclei due to p53 activation and nuclei translocation. Anti-p53 mouse monoclonal antibody was used to stain the cells and DAPI for nuclei. The scale bar is 10µm.

3.5.2. Quantification of p53 Upregulation Using Fluorescence Microscopy

In order to obtain solid evidence that the MN cell population undergoes stress that leads to the upregulation of p53 protein levels, I quantified the fluorescence of p53 protein in images of these cells. After staining procedure and sample preparaiton of the WT HEK293T and H60 cells, tile scans and z stacks was taken with the confocal microscope and maximum intensity projections and nuclei selections was made using ImageJ software. the quantification procedure is explained in detail in the methods section 2.2.7.

As a positive control for p53 upregulation, I used the HCT116 colon cancer cells. Two different anticancer drugs were used to induce DNA damage which leads to p53 levels upregulation. The first drug was Doxorubicin 2μM for 16 hours and the second drug was Cisplatin 50μM for 16 hours. I selected approximately 250 cells from each group (the untreated cells, Doxorubicin treated cells and Cisplatin treated cells). Data was plotted as a dot graph, the CTCF in Y axis and the area in X axis, and each dot in the graph represents one nucleus selection. I observed that the treated cells either with Doxorubicin or Cisplatin drugs, the CTCF levels were increased in comparison to the untreated cells (Fig. 3.17), this confirm the increase of p53 protein levels due to DNA damage.

 After that, I selected approximately 800 cells from each of the WT HEK293T and the NL cells, and 155 MN cells. Corrected Total Cell Fluorescence (CTCF) was calculated for each nuclei selection, then data was plotted as a dot graph. I observed that the MN cells showed increase in CTCF compared to WT HEK293T or NL cells. The CTCF Mean of the three cell types was also plotted as a bar graph that showed increase in the CTCF mean of the MN cells (Fig. 3.18).

This quantification experiment was repeated twice and both of these experiments confirm the previous immunofluorescence experiment and indicate that the MN cells are under stress that caused upregulation of p53. The possible causes and consequences of p53 upregulation in the MN cells are disscussed in the following sections.
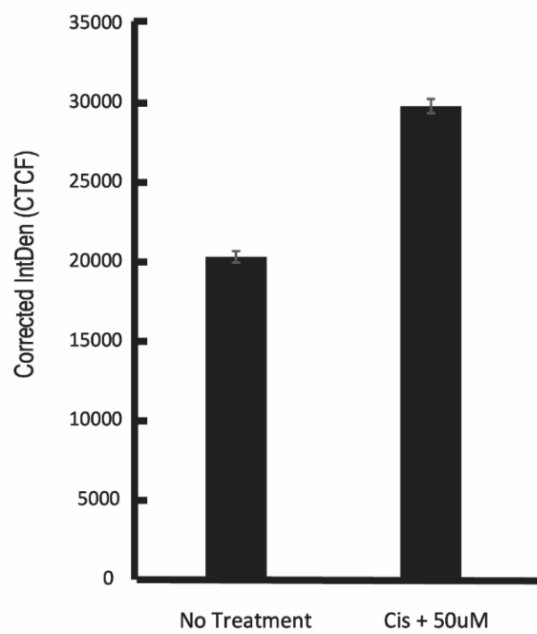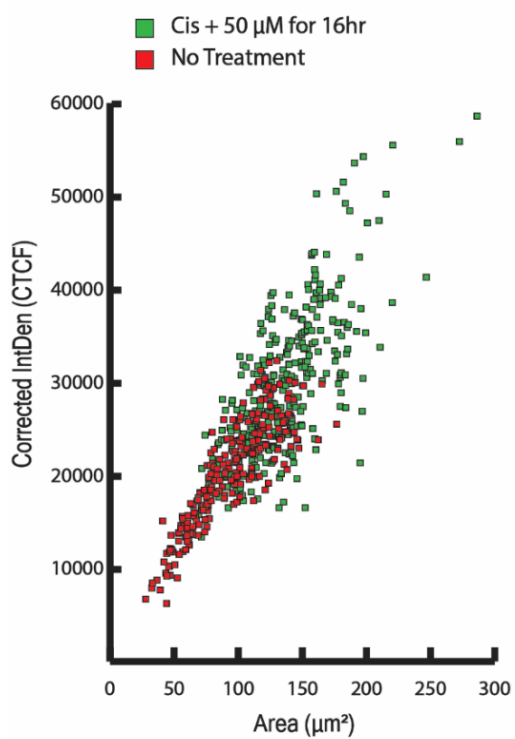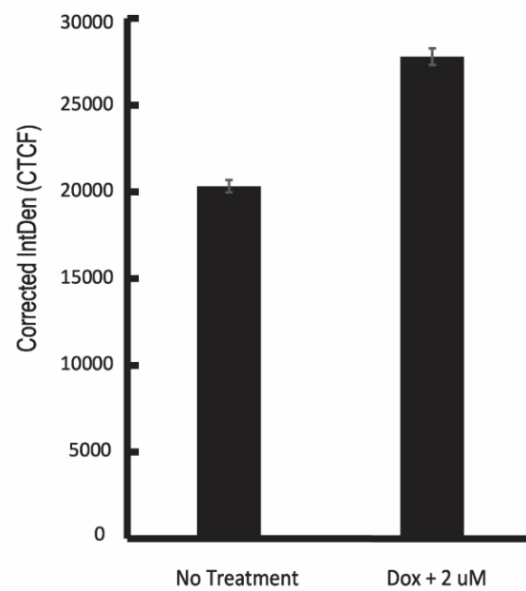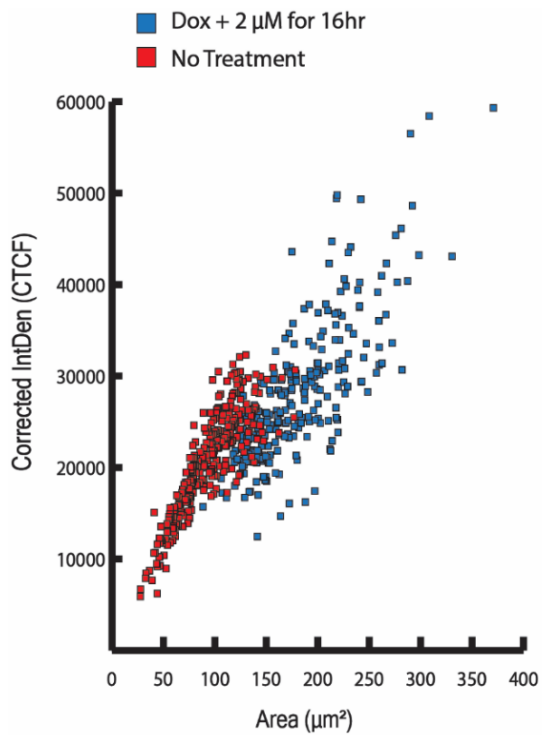
Figure 3.17 Quantification of p53 upregulation in HCT116 cells as a positive control

HCT116 cells were used as a positive control for the p53 quantification experiment. The cells were treated with two DNA damage inducing drugs, Doxorubicin and Cisplatin. After that the samples were fixed and processed for immunofluorescence with anti-p53 antibody and DAPI for nuclei. The quantification data shown in the graph was for 250 cells from each group the treated and the untreated cells. The corrected total cell fluorescence (CTCF) which was calculated and plotted in Y axis and the area of the selection in the X axis. (A) HCT116 cells were treated with 2 µM Doxorubicin for 16 hours. Doxorubicin increased p53 levels as a result of DNA damage. (B) HCT116 cells were treated with 50 µM Cisplatin, the levels of p53 is increased after 16 hour treatment. The graphs on the right represent the mean of the CTCF of the treated and the untreated cells.
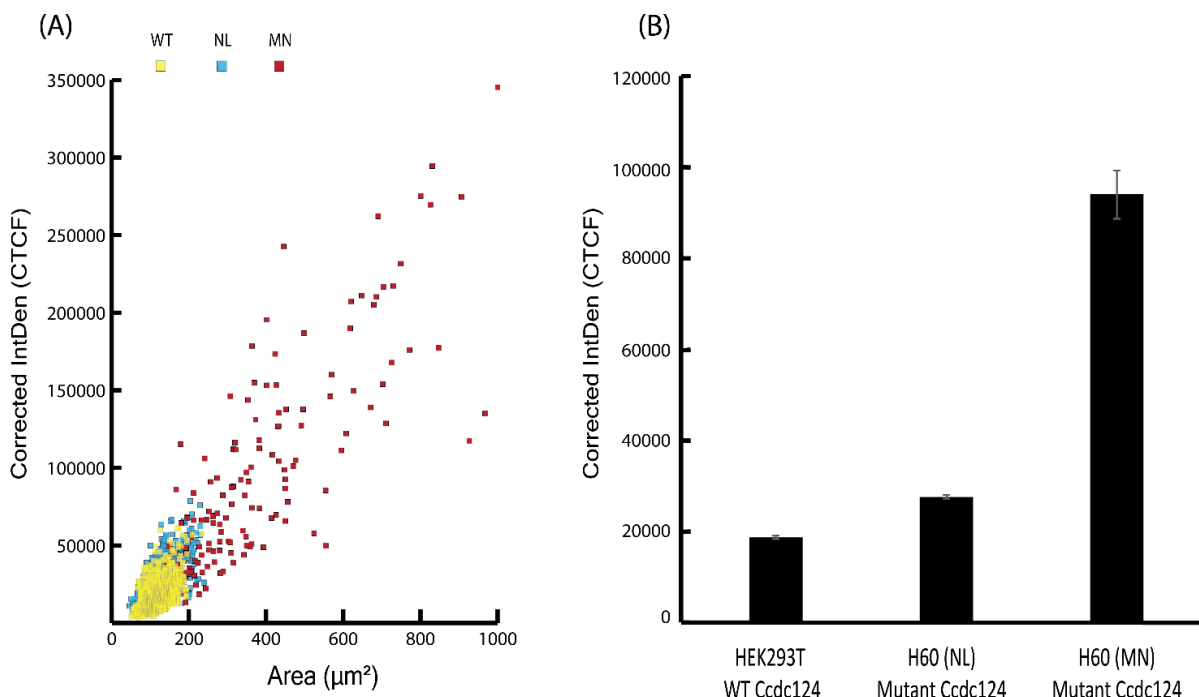
Figure 3.18 Upregulation of p53 in the MN cells

The WT HEK293T and H60 cells were fixed and processed for immunofluorescence with anti-p53 antibody and DAPI for nuclei. The quantification data shown in the graph was calculated from 155 of the MN cells, 800 from each of the WT HEK293T and the NL cells. After that, the background subtraction of the integrated density was made to calculate the corrected total cell fluorescence (CTCF). Each dot in the graph on the left represents quantification data of a single nucleus selection. (A) The MN cells showed increase in the CTCF in comparison to both the WT HEK293T and the NL cells. (B) The bar graph on the right represents the mean of the CTCF for each group and shows increase of the CTCF mean in the MN cells.

3.6. Senescence Associated β-Galactosidase Assay

After demonstrating that the MN cells had upregulated p53, I wanted to test the consequences of p53 activation. P53 can be a potential cause of cell cycle arrest which can be either a temporary or a permanent condition. Senescence is a permanent cell cycle arrest and senescent cells exhibit enlarged cell size, flattened morphology, inability to synthesize DNA but they are metabolically active. They express the β-galactosidase lysosomal enzyme in larger amounts than the normal cells which is a commonly used senescence biomarker and can be detected at pH6.0 (see methods section 2.2.8) by using the senescence associated β-galactosidase assay (SA-β-gal or SABG) [32]. A chromogenic X-gal substrate is used in this assay and results in production of blue-green stain in senescent cell.

When I performed the aforementioned senescence assay for both WT HEK293T and H60, I observed a blue-green stain in most of the MN cells which indicated that these cells are senescent (Fig. 3.19). The senescent cells were quantified and plotted as a bar graph (Fig.3.20).
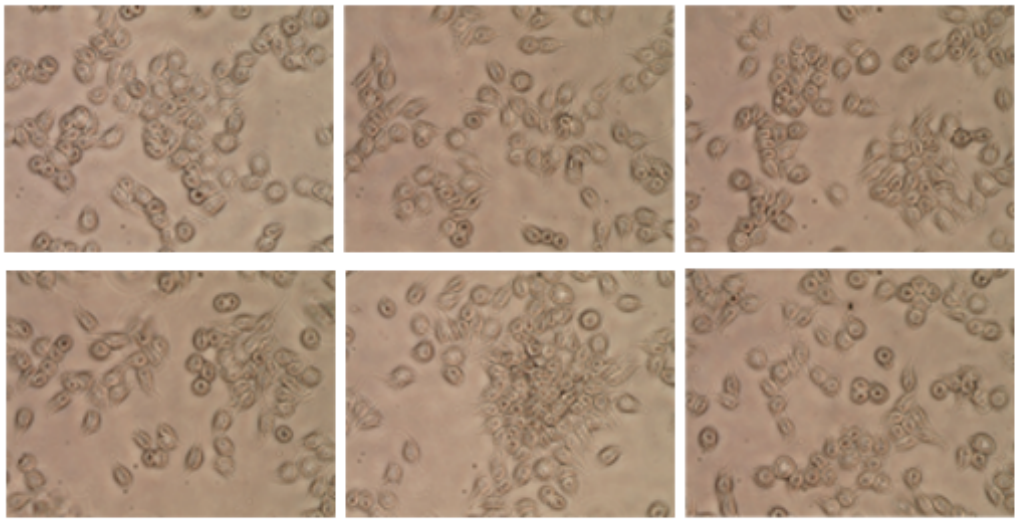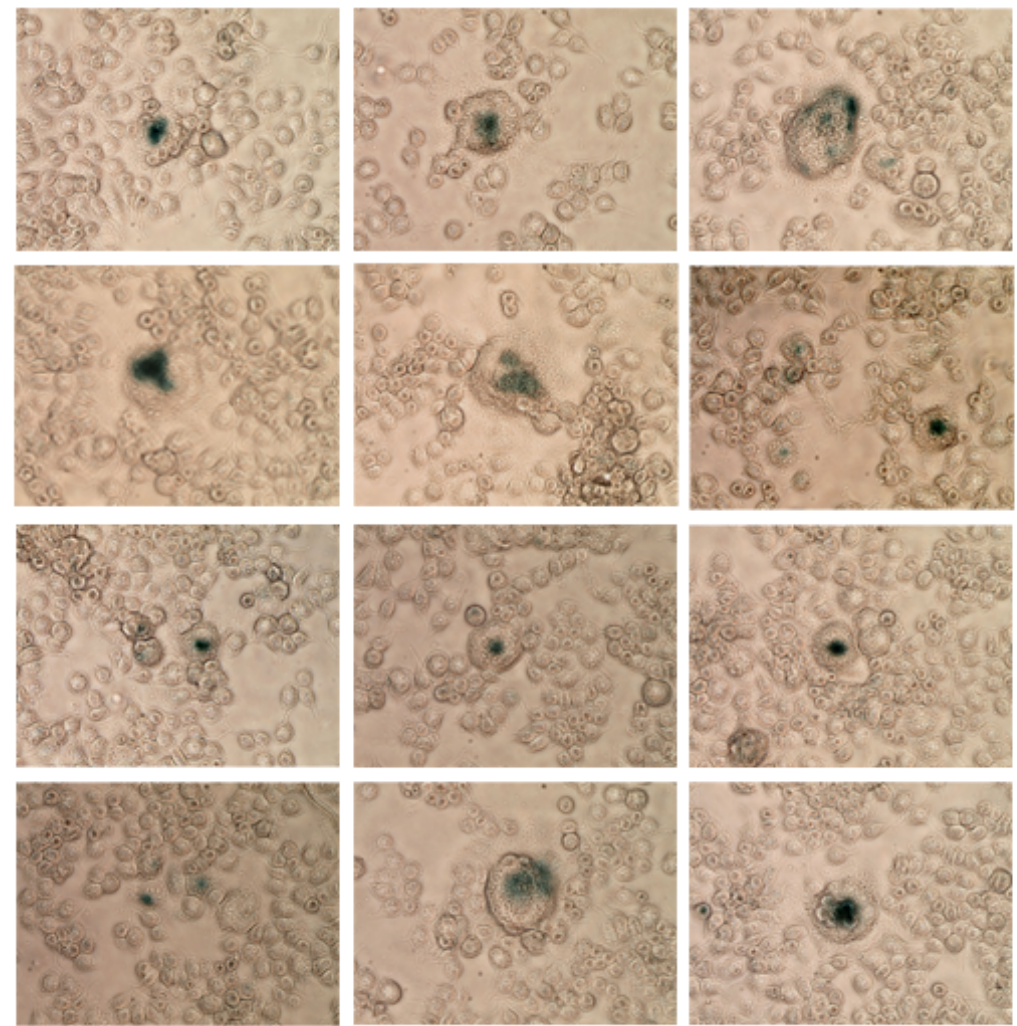
Figure 3.19 P53-induced senescence in the MN cells

Senescence associated β-galactosidase assay was performed by using the chromogenic X-gal substrate that produce blue-green color in the senescent cells. Most of the MN cells had the blue-green stain which indicate that they are senescent.
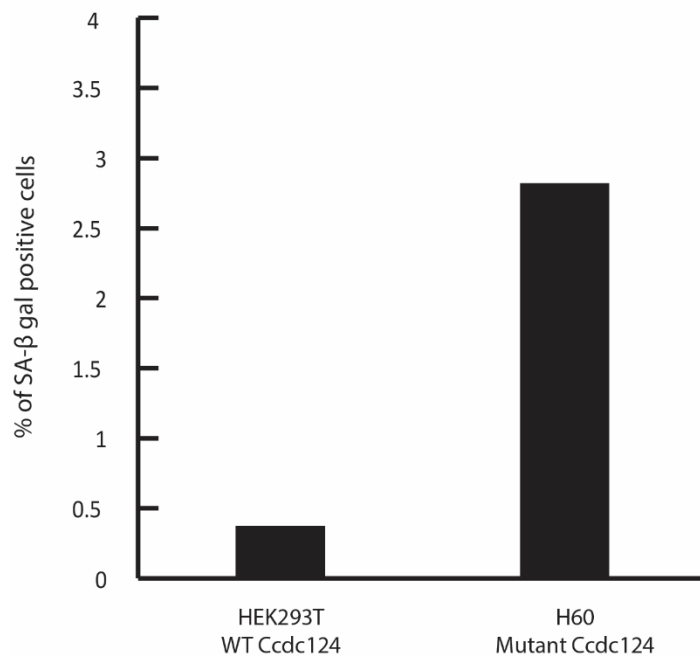
Figure 3.20 Quantification of senescent cells

Five hundred cells were counted from each H60 and the WT HEK293T cells then the percentage of the senescent cells were calculated and plotted in the bar graph. The H60 cells have more senescent cells in which most of them were among the MN cells.

3.7. 53BP1 Foci Formation in the MN cells

A possible cause of the upregulation of p53 in the MN cells could be the initiation of the DNA damage response (DDR) pathway that can be initiated by chromosome and mitotic errors. Several factors can cause DNA double strand breaks such as reactive oxygen species (ROS), ionizing radiation (IR), ultraviolet (UV) light or cytotoxic agents. Recent studies demonstrated that aberrations during mitosis could also lead to direct and indirect damage of DNA and chromosome breaks[33].

The DDR is initiated when DNA double strand breaks (DSBs) are detected, this activates a number of proteins to mark the site of the break and recruit more repair proteins to the site of the damage. One of these proteins is the 53BP1 (53 binding protein 1) that is recruited to the DSBs and form foci that can be detected by immunofluorescent staining. 53BP1 foci was observed to be increased in cells that are exposed to gamma radiation which induces DNA DSBs, the foci number was increased by higher doses of radiation or longer cell exposure. To test whether the DDR is activated in H60 MN cells, I performed immunofluorescence staining of the WT HEK293T and H60 cells with an anti-53BP1 rabbit antibody. Analysis of 53BP1 immunofluorescence images acquired on the confocal microscope showed that the number of 53BP1 foci was dramatically increased in most of the MN cells, compared to the WT HEK293T and the H60 NL cells. Moreover, the size of some of these foci was also larger in the MN cells compared to those in the NL cells (Fig.3.21). This suggested that p53 upregulation in the MN cells is potentially a part of the DDR induced by mitotic stress. Other possible pathways of p53 upregulation in the MN cells were not investigated in this study and remain interesting avenues for further research.
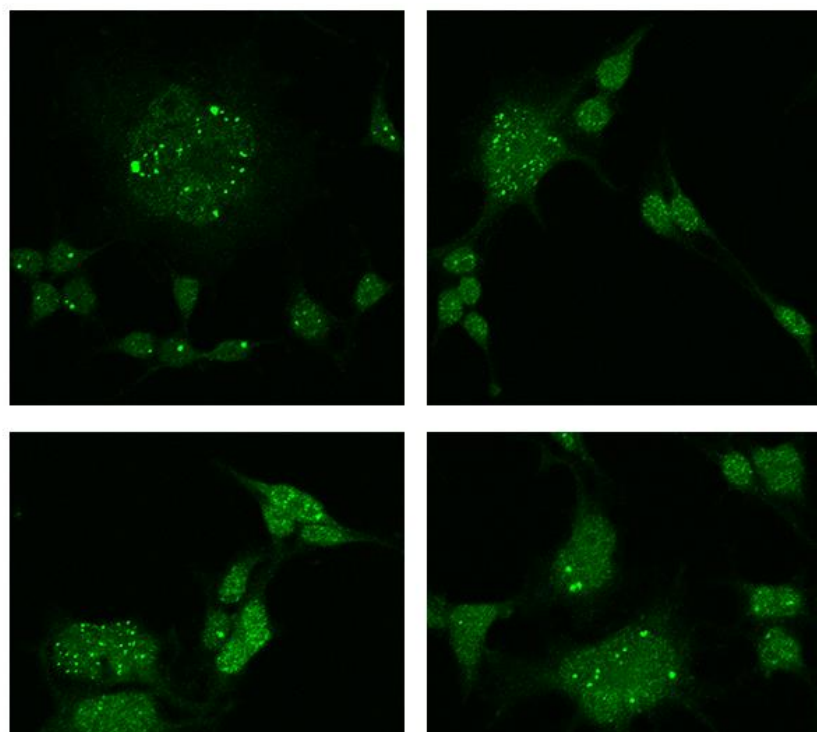
WT HEK293T
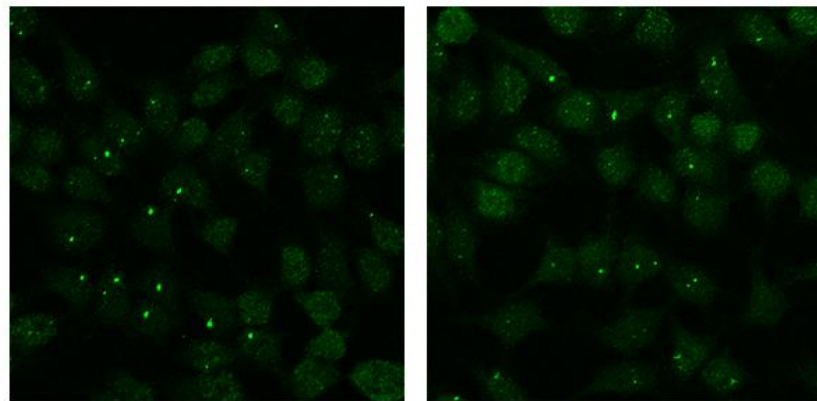
H60

Figure 3.21 53BP1 foci formation as an indication of DNA damage in the MN cells

HEK293T and H60 cells were stained with anti-53BP1 rabbit antibody. 53BP1 foci formation are an indication of DNA damage. Increased number of the 53BP1 foci was observed in the MN cells, some of them was had large foci size compared to the WT HEK293T cells.

4. DISCUSSION AND CONCLUSION

The Ccdc124 protein was identified as a novel centrosome and midbody protein and it is a pericentriolar material (PMC) protein that is colocalized with the major centrosome protein gamma-tubulin. This colocalization is evident when the cell is in interphase or during mitosis after which Ccdc124 relocates to the midbody region at cytokinesis where the intercellular bridge between the two daughter cells is resolved[14]. This localization was observed in HeLa cells and in the current study, I confirmed the same results in HEK293T wild type cells by immunofluorescent staining. When the Ccdc124 protein was knocked down with siRNA in HeLa cells[14] or mutated in HEK293T cells[15], multinucleated aberrant cells were formed, a phenotype which underlines the important role of the Ccdc124 protein in cytokinesis at the end of mitosis. In the current study, I analyzed in detail the multinucleated cells that were observed in the Ccdc124 mutant clone H60 using flow cytometry, immunofluorescence by confocal microscopy and image analysis techniques.

I found that the H60 clone has two cell populations, normal-looking (NL) and he multinucleated cells (MN). Even though NL cells have almost the same phenotype as the WT HEK293T, their genotype is different (according to sequencing results). Interestingly, even though MN cells have the same genotype as the NL cells, they have a dramatically different phenotype. In NL cells, Ccdc124 protein is colocalized to a focus structure with gamma-tubulin in interphase and in mitosis in the midbody during cytokinesis. The presence of Ccdc124 protein in NL cells can be explained by the fact that Ccdc124 protein still can be produced from the allele that has only a 24 nucleotide deletion (Fig. 1.9). While the precursor product relationship between NL and MN cells has not been determined, it is likely that NL cells are the precursors of MN cells. I hypothesize that at a certain point, NL cells gave rise to the MN cells that attain a terminal phenotype that is totally different than either the NL or the WT HEK293T cells. Currently, the factor that triggers this process is

unknown, however I hypothesize that this factor may be the accumulation of an unknown stress factor. Alternatively, a threshold in the number of cell divisions that NL cells undergo could be affecting this process.

MN cells have accumulated nuclei (aneuploidy; the state of having an abnormal chromosome number) due to a failure of cytokinesis in which cells continue dividing the DNA material but fail to separate their cytoplasm (endoreduplication). Nuclei accumulation could lead to a massive increase in the cell size with time, in which a single MN cell could reach more than 70 μm in diameter as I observed in the cell culture (Fig. 3.1). This aneuploid phenotype of the MN cells is stable (the H60 clone was established in our lab and cultured for more than 6 months).

The immunofluorescence analysis of the MN cells has revealed more about the phenotype and mitotic stages of these cells. I found that the MN cells have multiple centrosomes or supernumerary centrosomes (centrosome amplification) which could be a result of cytokinesis failure in these cells. It is known that centrosome amplification takes place when a cell have more than two centrosomes, and they occur due to different abnormalities, such as cell division failure, cell fusion and centrosome overduplication[23,34]. Formation of extra centrosomes is usually found in human tumour cells and their presence is mostly associated with aneuploidy[34]. Moreover, supernumerary centrosomes were identified in the early developmental stages of some haematological and solid tumours, and has been demonstrated to be connected with proliferation rate, tumour grade, and the degree of genome instability[35,36].

In interphase, the MN cells contain multiple centrosomes that made clusters mainly in the center of the cell, between the multiple nuclei. The Ccdc124 protein colocalized with gamma-tubulin in these multiple centrosomes as seen in (Fig.3.4). In a previous study, it was demonstrated that multiple daughter centrioles form around one mother centriole which creates multiple centrosomes in the next cell cycle[34]. It was proposed that cells with supernumerary centrosomes use centrosome clustering as an adaptation mechanism to avoid lethal multipolar divisions[25].

In prophase, chromosomes started to condense and multiple centrosomes were observed in the MN cells, unlike the NL or WT HEK293T cells that have only two centrosomes during

this phase as a result of duplication of one centrosome in the cell (Fig.3.5). The NL and WT HEK293T cells had normal metaphase and anaphase due to the formation of bipolar mitotic spindles that led to correct chromosome alignment at the equator of the cell in metaphase and proper chromosome segregation in anaphase. In contrast, the MN cells had aberrations in chromosome alignment. Instead of alignment in the center of the cell, they were aligned in multiple metaphase plates because they have supernumerary centrosomes that formed multipolar mitotic spindles which likely caused defects of chromosome alignment and multipolar divisions in anaphase (Fig.3.6 and 3.7).

The formation of multipolar mitotic spindles in MN cells during metaphase caused defects in chromosome alignment and chromosome missegregation in anaphase. The observation of lagging chromosomes and monotelic chromosomes is consistent with these chromosomal misalignment defects (Fig.3.10 and 3.11). It was previously demonstrated that extra centrosomes caused the assembly of multipolar mitotic spindles and led to catastrophic chromosome missegregation[37,38]. Similar defects were found in aneuploid tumour cells that have chromosome instability (CIN) (a status in which cells are incapable to properly segregate whole chromosomes (whole CIN [W-CIN]) or liable to structural chromosome rearrangements (structural CIN [S-CIN]), such as translocations, deletions, and duplications of some parts of chromosomes)[39]. CIN is the most consistent characteristics of human solid tumors[40], however, the underlying cause of increased malorientations in the CIN cells has not been identified yet, but can originate from errors in spindle assembly[34] or the regulation of kinetochore-microtubule attachment[26]. In addition, CIN was demonstrated to cause aneuploidy but it is not necessarily generated by aneuploidy itself as a previous study showed that not all aneuploid cells exhibit CIN[23].

In earlier studies, CIN was related to mutations of set of genes in which their expression was disturbed in certain types of cancer[40]. These genes were identified to be involved mainly in cell cycle check point, DNA replication and repair, mitotic spindle formation, spindle assembly checkpoint (SAC), centrosome integrity, chromosome condensation and segregation, or cytokinesis[40]. The Ccdc124 gene mutation in H60 cells could be a direct or an indirect cause of CIN in the MN cells. Usually CIN related genes were overexpressed in cancer and Ccdc124 protein was found to be overexpressed in certain types of cancer as

well[41,42], so I hypothesized that Ccdc124 can be one of the CIN causing genes. Furthermore, the aneuploidy that was associated with CIN in H60 MN cells could support this hypothesis. The mechanism that mutation of Ccdc124 could cause CIN in the MN cells might be related to centrosome amplification that was evident in the MN cells during mitosis.

The presence of multiple centrosomes in the MN cells were related to cytokinesis failure and subsequent replication of centrosomes that was associated with endoreduplication of nuclei. Centrosome amplification caused multipolar spindle formation, centrosome clustering, mitotic and chromosome attachment errors and subsequent micronuclei formation. Some centrosomal proteins were identified to cause centrosome amplification if overexpressed, it is not confirmed yet if overexpression of Ccdc124 protein can cause centrosome amplification (de novo centriole generation), in this case Ccdc124 protein might be related to centrosome biogenesis or centrosome duplication cycle. More investigation is needed to determine if the CIN associated with Ccdc124 mutation was caused by centrosome amplification alone or whether the Ccdc124 protein might be involved in other pathways or mitosis checkpoints such as spindle assembly checkpoint (SAC).

SAC prevents cells from separating their sister chromatids and exiting mitosis until all kinetochores are connected to the spindle. A single unattached kinetochore can delay cells in mitosis for hours[43]. SAC is activated by lack of kinetochore–microtubule attachments[44] so if there are any disturbances in this pathway the monotelic chromosomes (only one kinetochore is attached to one spindle pole) can be undetected and the cell proceed to anaphase which eventually leads to chromosome missegregation. Even though the MN cells have significant amount of unaligned chromosomes (Fig.3.11), cells were continuously undergoing endoreduplication and exit mitosis. This can indicate the presence of unregulated SAC in the MN cells that could be related directly or indirectly to Ccdc124 mutation. More investigation is needed to demonstrate if the unaligned chromosomes in the MN cells are monotelic, syntelic (both sister kinetochores are attached to the same spindle pole) (Fig. 4.1) or whether they remained unattached to any of the spindle poles. This can

be detected using immunofluorescence staining against both kinetochores and microtubules in the MN cells.
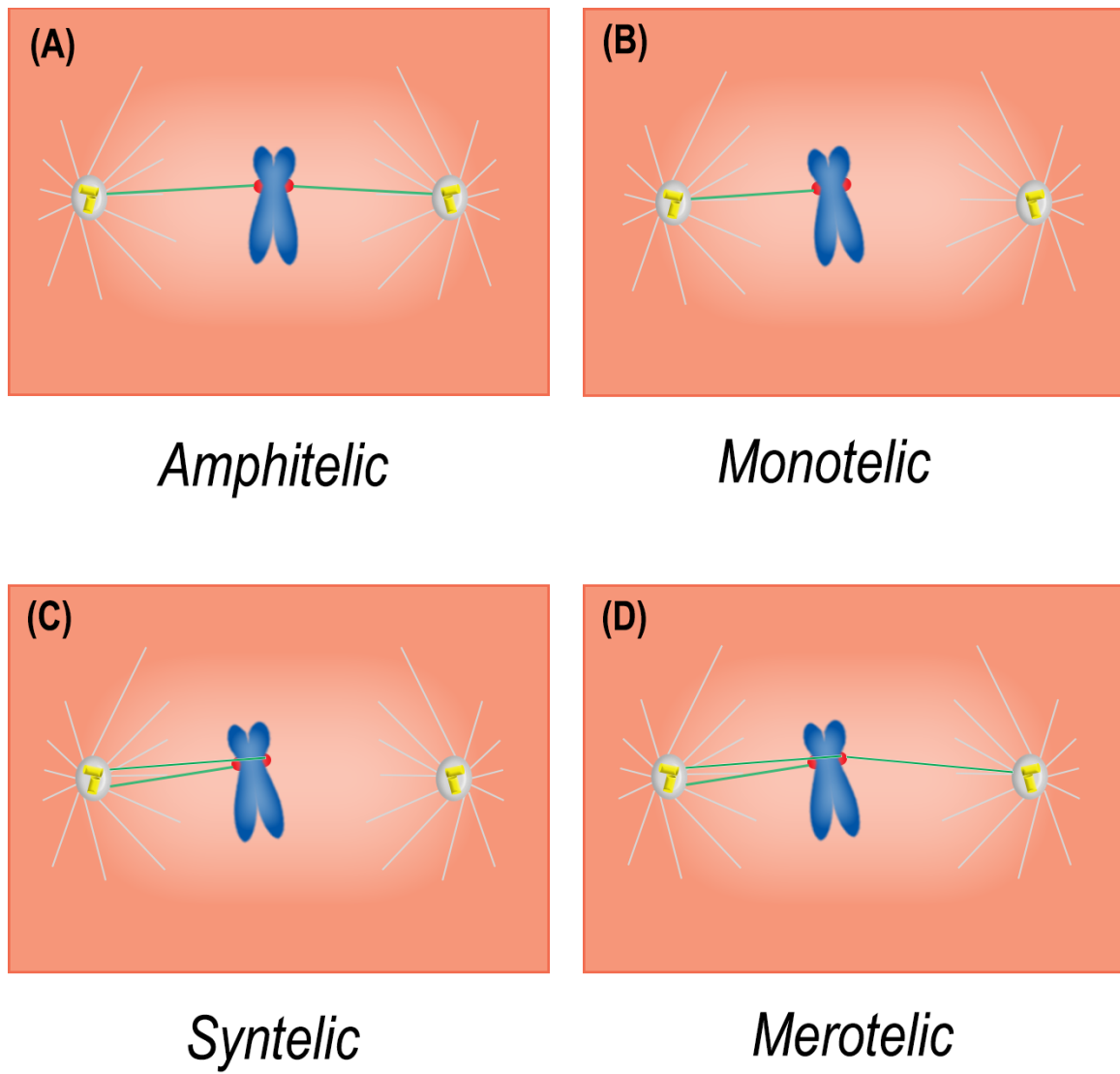
Figure 4.1 Types of kinetochore-microtubule attachment

(A) Amphitelic: bipolar or bioriented attachment (the normal chromosome attachment). Sister kinetochores bind only to microtubules arising from the adjacent spindle pole. (B) Syntelic: sister kinetochores attach to microtubules emanating from the same spindle pole. (C) Monotelic: only one kinetochore binds microtubules, leaving an unattached kinetochore. (D) Merotelic: one (or both) kinetochore(s) attach to microtubules from both poles.

At telophase, the cleavage furrow started to form and the Ccdc124 protein was recruited to the midbody region in the NL and WT HEK293T cells during cytokinesis. However, MN cells behave differently whereby they form daughter nuclei after anaphase and they can undergo endoreduplication. Currently, the cause of this defect in MN cells is not known. In fact, the presence of stabilized p53 protein in the HEK293T cell line that was used to create the H60 clone can be a potential cause of continuous endoreduplication in the MN cells in which cells continue to grow with a low rate of apoptosis. HEK 293T cells expresses a temperature-sensitive allele of the SV40 T antigen[45]. While this is advantageous for using these cells to harbor multicopy vectors containing the SV40 origin of replication in transient transfections, but the presence of SV40 T makes studying p53 dependent effects in these cells difficult. SV40 T forms a complex with and inhibits p53, possibly further compromising genome integrity[46]. Furthermore, other viral proteins such as adenovirus early region 1A and 1B (E1A/E1B) are expressed in HEK293T cells. They upregulate and bind to p53 directly such that it is transcriptionally inactivated which leads to an interference with the cell cycle pathways and counteract apoptosis[45,47].

Alternative reasons for the continuous endoreduplication of MN cells could be the dysfunction of telomeres which in previous studies was associated to the formation of tetraploid cells. The continuous proliferation of eukaryotic cells with deficiency of telomerase activity can cause gradual shortening of telomeres which leads finally to the exposure of uncapped chromosome ends. It was demonstrated that two unprotected telomere ends can fuse together to form a dicentric chromosome with two kinetochores. If the two kinetochores of the dicentric chromosomes are pulled towards opposite mitotic poles during mitosis the resulting lagging chromosome can lead to cytokinesis failure. Moreover, the unprotected telomere ends cause a continuing DNA damage signal that might enhance endoreduplication in p53-deficient cells. In addition, short telomeres are frequently observed in cancer cells before telomerase reactivation, temporary telomere dysfunction can be an essential cause of tetraploidization in human tumours[23]. Further investigations are needed to determine the cause of continuous endoreduplication in MN cells.

The p53 pathway has an essential role in restriction of the propagation of aneuploid cells in culture to maintain the diploid karyotype of the population and the experimentally created tetraploid cells encounter a p53-dependent cell cycle arrest[27,28,30]. Consistently, the p53 fluorescence quantification data showed an upregulation of p53 which caused the p53-dependent senescence in the MN cells (Fig. 3.18 and 3.20). In fact, the p53 pathway activation is also thought to take pleace in other circumstances of tetraploidization, but the process guiding this phenomenon is not fully identified. The p53 pathway could be activated by tetraploidy or by the presence of extra centrosomes[48,26].

In order to investigate the p53 activation pathway in the MN cells, I checked the DNA damage response (DDR) pathway that cause the formation of 53BP1 foci. This was addressed in a study that linked abnormal mitosis and chromosomal instability (CIN) to DNA damage, where it was demonstrated that in anaphase, lagging chromosomes undergo a microtubule-generated pulling force that is strong enough to lead to the extreme physical stretching and deformation of their kinetochores and the associated DNA near the centromeres[22,49]. We observed that the MN cells had increased numbers of chromosome attachment errors and lagging chromosome formation at anaphase (Fig. 3.10). Moreover, these cells have more 53BP1 foci in comparison to the NL or the WT HEK293T cells (Fig.3.21). Other possible causes of the activation of the p53 pathway the MN cells are telomere shortening, mitochondria and ROS formation. P53-dependent senescence was linked to dysfunctional telomeres (shortened telomeres or an altered telomere state) in senescent cells[50,51]. Another important cause of senescence, at the molecular level, is the oxidative damage accumulation intracellularly due to production of reactive oxygen species (ROS). ROS are mostly small, short-lived and very reactive molecules and senescence was associated to ROS-mediated damage to macromolecules such as nucleic acids, proteins and lipids. Mitochondria are the major source of ROS and accumulation of defective mitochondria increase ROS formation and subsequent oxidative damage to the cell which can induce senescence[52] (Fig. 4.2).

The HEK293T H60 clone is a valuable cell line that can be used to study mitotic defects and chromosome aberrations, centrosome clustering and chromosomal instability that are

reported to occur frequently in tumour cells. Furthermore, the H60 cell line can be used to test drugs that target centrosomal clustering in tumour cells.

Considering all the results of this study, I prepared a model to show the relationship between the Ccdc124 mutation-associated cytokinesis failure that results in the formation of aneuploid cells and the induction of subsequent p53-associated senescence. (Fig. 4.3).
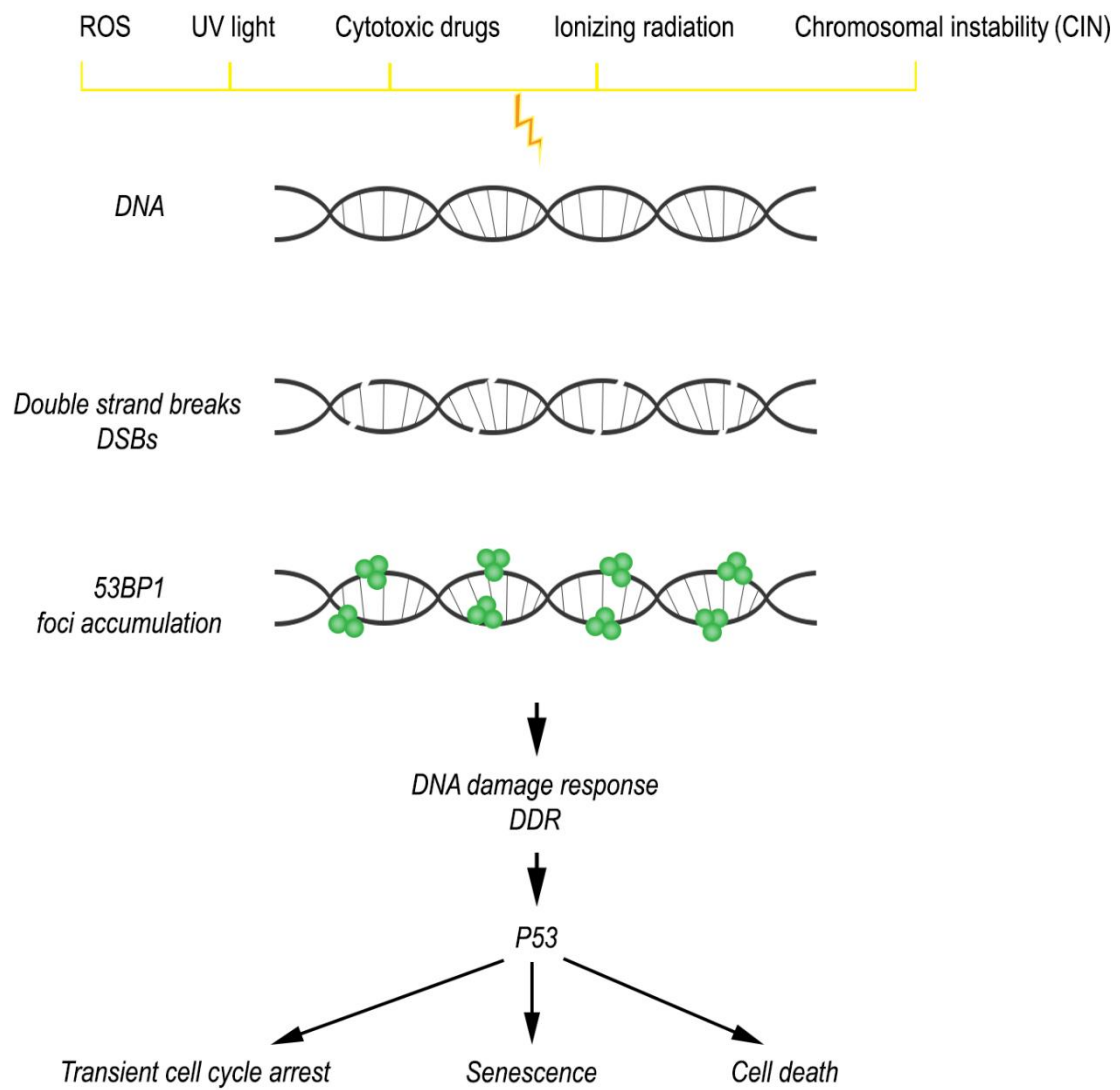
Figure 4.2 DNA damage response (DDR)

Chromosomal instability (CIN) leads to formation of DNA damage and double strand breaks which cause accumulation of 53BP1 foci and activation of DNA damage response (DDR) then subsequent p53 upregulation that can lead to different outcomes such as transient cell cycle arrest, senescence or cell death.
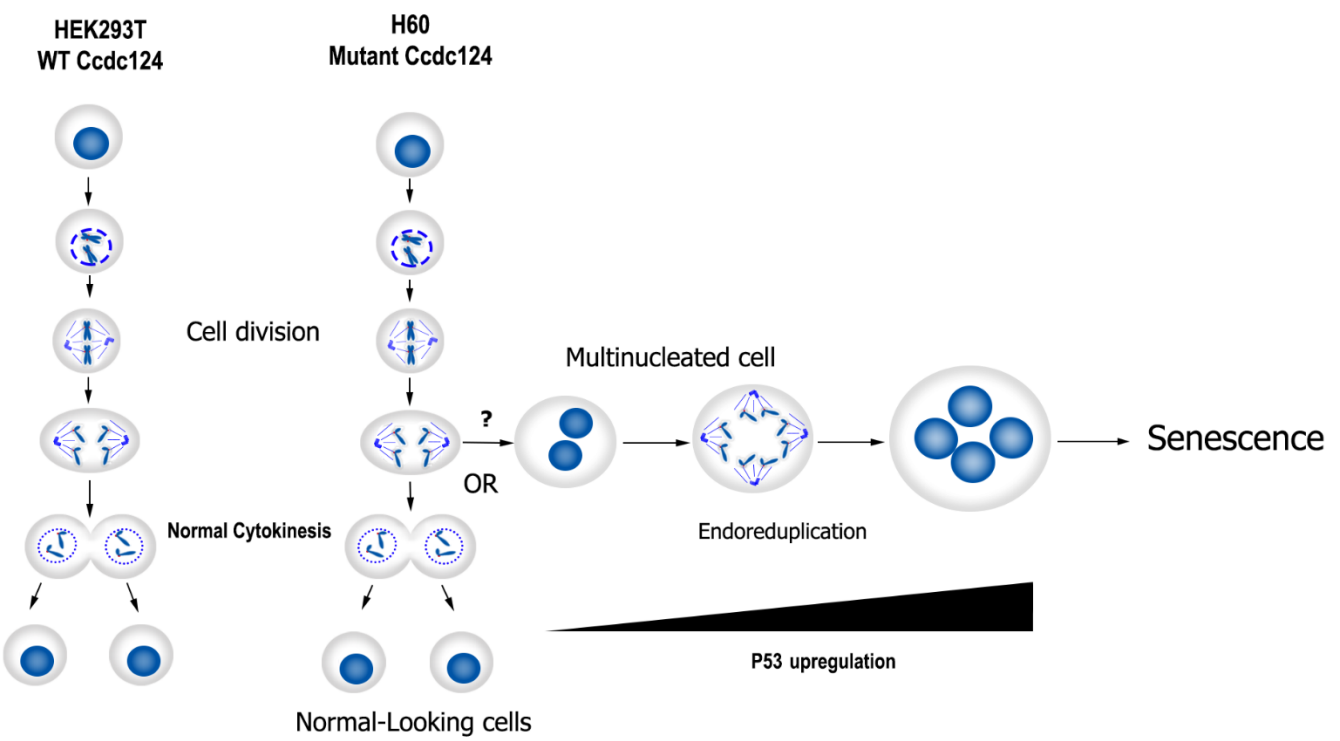
Figure 4.3 Ccdc124 gene mutation leads to the formation of aneuploid cells and subsequent senescence

In this model, the mutation of the Ccdc124 protein induced cytokinesis failure and resulted in the formation of aneuploid cells and the subsequent formation of p53 related senescence.

APPENDIX

APPENDIX A: Chemicals Used In The Study

Chemicals and Media Components	Supplier Company
Acetic Acid	Merck, Germany
Bovine Albumin Fraction V (BSA)	MP Biomedicals, USA
Distilled water	Milipore, France
DMEM	PAN, Germany
DMSO	Sigma, Germany
Ethanol	Riedel-de Haen, Germany
Fetal Bovine Serum (FBS)	Biological Industries, Germany
HBSS	CellGro, USA
Hydrochloric Acid	Merck, Germany
Isopropanol	Riedel-de Haén, Germany
Liquid nitrogen	Karbogaz, Turkey
Magnesium Chloride	Merck, Germany
Methanol	Riedel-de Haen, Germany
Nocodazole	Sigma, Germany
PBS	Sigma, USA
Penicillin-Streptomycin	Sigma, Germany
Poly-L-lysine solution	Sigma, USA
Potassium ferrocyanide	Merck, Germany

Potassium ferricyanide trihydrate	Merck, Germany
RNase A	Roche, Germany
Sodium Azide	Amresco, USA
Sodium Chloride	Amresco, USA
Sodium hydroxide	Sigma, Germany
Sodium phosphate dibasic heptahydrate	Sigma, Japan
Thymidine	Sigma, China
Triton X-100	Sigma, USA
X-Gal (5-bromo-4-chloro-3-indolyl-beta-D-galacto-pyranoside)	AppliChem GmbH, Germany

APPENDIX B: Equipment Used In The Study

Equipment	Company
Autoclave	Hirayama,Hiclave HV-110,Japan
Balance	Sartorius, BP221S, Germany
	Schimadzu, Libror EB-3200 HU, Japan
Cell Counter	Cole Parmer, USA
Centrifuge	Eppendorf, 5415D, Germany
CO2 Incubator	Binder,Germany
Deepfreeze	-80ºC, Forma,Thermo ElectronCorp.,USA
	-20ºC, Bosch,Turkey
Distilled Water	Millipore, Elix-S, France
Flow Cytometer	BDFACSCanto,USA
Hematocytometer	Hausser Scientific,Blue Bell Pa.,USA
Ice Machine	Scotsman Inc., AF20, USA
Incubator	Memmert, Modell 300, Germany
	Memmert, Modell 600, Germany
Kamerams CMOS camera	ARGENIT LTD, Turkey
Laminar Flow	Kendro Lab. Prod., Heraeus, HeraSafe HS12, Germany
Liquid Nitrogen Tank	Taylor-Wharton,3000RS,USA
Magnetic Stirrer	VELP Scientifica, ARE Heating Magnetic Stirrer, Italy

Microliter Pipettes	Gilson, Pipetman, France
	Eppendorf, Germany
Microscope	Olympus CK40,Japan
	Olympus CH20,Japan
	Olympus IX70,Japan
	Zeiss Confocal LSM710, German
PH meter	WTW, pH540 GLP MultiCal, Germany
Power Supply	Biorad, PowerPac 300, USA
Refrigerator	Bosch,Turkey
Vortex	Velp Scientifica,Ital

REFERENCES

1. Bettencourt-Dias, M. & Glover, D. M. Centrosome biogenesis and function: centrosomics brings new understanding. *Nat. Rev. Mol. Cell Biol.* 8, 451–463 (2007).

2. Urbani, L. The centrosome. 315–317

3. Wang, G., Jiang, Q. & Zhang, C. The role of mitotic kinases in coupling the centrosome cycle with the assembly of the mitotic spindle. *J. Cell Sci.* 1–12 (2014). doi:10.1242/jcs.151753

4. Dionne, L. K., Wang, X.-J. & Prekeris, R. Midbody: from cellular junk to regulator of cell polarity and cell fate. *Curr. Opin. Cell Biol.* 35, 51–8 (2015).

5. Hu, C.-K., Coughlin, M. & Mitchison, T. J. Midbody assembly and its regulation during cytokinesis. *Mol. Biol. Cell* 23, 1024–1034 (2012).

6. Steigemann, P. & Gerlich, D. W. Cytokinetic abscission: cellular dynamics at the midbody. *Trends Cell Biol.* 19, 606–616 (2009).

7. Foe, V. E. & von Dassow, G. Stable and dynamic microtubules coordinately shape the myosin activation zone during cytokinetic furrow formation. *J. Cell Biol.* 183, 457–70 (2008).

8. Enjalbert, B. *et al.* Role of the Hog1 stress-activated protein kinase in the global transcriptional response to stress in the fungal pathogen Candida albicans. *Mol. Biol. Cell* 17, 1018–1032 (2006).

9. Terada, Y. *et al.* AIM-1: a mammalian midbody-associated protein required for cytokinesis. *EMBO J.* 17, 667–76 (1998).

10. Gromley, A. *et al.* Centriolin anchoring of exocyst and SNARE complexes at the midbody is required for secretory-vesicle-mediated abscission. *Cell* 123, 75–87 (2005).

11.   Schulze, E. S. & Blose, S. H. Passage of molecules across the intercellular bridge between post-mitotic daughter cells. *Exp. Cell Res.* 151, 367–373 (1984).

12.   Toes, R. E. *et al.* References and Notes 1. 331, (2011).

13.   Pohl, C. & Jentsch, S. Midbody ring disposal by autophagy is a post-abscission event of cytokinesis. *Nat. Cell Biol.* 11, 65–70 (2009).

14.   Telkoparan, P. *et al.* Coiled-Coil Domain Containing Protein 124 Is a Novel Centrosome and Midbody Protein That Interacts with the Ras-Guanine Nucleotide Exchange Factor 1B and Is Involved in Cytokinesis. *PLoS One* 8, e69289 (2013).

15.   GÜL, Sinem (Gebze Teknik Üniversitesi, M. B. and G. department). *The effects of a deletion muation on Ccdc124 using CRISPER/Cas9 system*. (2015).

16.   Lee, S. *et al.* Global mapping of translation initiation sites in mammalian cells at single-nucleotide resolution. *Proc. Natl. Acad. Sci.* 109, E2424–E2432 (2012).

17.   Epting, D., Vorwerk, S., Hageman, A. & Meyer, D. Expression of rasgef1b in zebrafish. *Gene Expr. Patterns* 7, 389–395 (2007).

18.   Yaman, E., Gasper, R., Koerner, C., Wittinghofer, A. & Tazebay, U. H. RasGEF1A and RasGEF1B are guanine nucleotide exchange factors that discriminate between Rap GTP-binding proteins and mediate Rap2-specific nucleotide exchange. *FEBS J.* 276, 4607–4616 (2009).

19.   Andrade, W. a *et al.* Early endosome localization and activity of RasGEF1b, a toll-like receptor-inducible Ras guanine-nucleotide exchange factor. *Genes Immun.* 11, 447–57 (2010).

20.   Schiel, J. A. & Prekeris, R. Membrane dynamics during cytokinesis. *Curr. Opin. Cell Biol.* 25, 92–98 (2013).

21.   F Ann Ran, Patrick D Hsu, Jason Wright, Vineeta Agarwala, D. A. S. & F. Z. Genome engineering using the CRISPR-Cas9 system. *Nature* 8, 2281–2308 (2013).

22.   Maiato, H. & Logarinho, E. Mitotic spindle multipolarity without centrosome amplification.

Nat. Cell Biol. 16, 386–94 (2014).

23. Holland, A. J. & Cleveland, D. W. Losing balance: the origin and impact of aneuploidy in cancer. *EMBO Rep.* 13, 501–514 (2012).

24. Fenech, M. *et al.* Molecular mechanisms of micronucleus, nucleoplasmic bridge and nuclear bud formation in mammalian and human cells. *Mutagenesis* 26, 125–132 (2011).

25. Krämer, A., Maier, B. & Bartek, J. Centrosome clustering and chromosomal (in)stability: A matter of life and death. *Mol. Oncol.* 5, 324–335 (2011).

26. Davoli, T. & de Lange, T. The Causes and Consequences of Polyploidy in Normal Development and Cancer. *Annu. Rev. Cell Dev. Biol.* 27, 585–610 (2011).

27. Andreassen, P. R., Lohez, O. D., Lacroix, F. B. & Margolis, R. L. Tetraploid state induces l-dependent arrest of nontransformed mammalian cells in G1. *Mol. Biol. Cell* 12, 1315–1328 (2001).

28. Meraldi, P., Honda, R. & Nigg, E. a. Aurora-A overexpression reveals tetraploidization as a major route to centrosome amplification in p53-/- cells. *EMBO J.* 21, 483–492 (2002).

29. Brooks, C. L. & Gu, W. New insights into p53 activation. *Cell Res.* 20, 614–621 (2010).

30. Thompson, S. L. & Compton, D. A. Proliferation of aneuploid human cells is limited by a p53-dependent mechanism. *J. Cell Biol.* 188, 369–381 (2010).

31. Ganem, N. J. *et al.* Cytokinesis Failure Triggers Hippo Tumor Suppressor Pathway Activation. *Cell* 158, 833–848 (2014).

32. Lee, B. Y. *et al.* Senescence-associated beta-galactosidase is lysosomal beta-galactosidase. *Aging Cell* 5, 187–95 (2006).

33. Ganem, N. J. & Pellman, D. Linking abnormal mitosis to the acquisition of DNA damage. *J. Cell Biol.* 199, 871–881 (2012).

34. Holland, A. J. & Cleveland, D. W. Boveri revisited: chromosomal instability, aneuploidy and tumorigenesis. *Nat. Rev. Mol. Cell Biol.* 10, 478–487 (2009).

35. Chng, W. J. *et al.* Clinical implication of centrosome amplification in plasma cell neoplasm.

Blood 107, 3669–3675 (2006).

36.   Yamamoto, Y. *et al.* Centrosome hyperamplification predicts progression and tumor
        recurrence in bladder cancer. *Clin. Cancer Res.* 10, 6449–55 (2004).

37.   Silkworth, W. T., Nardi, I. K., Scholl, L. M. & Cimini, D. Multipolar spindle pole
        coalescence is a major source of kinetochore mis-attachment and chromosome mis-
        segregation in cancer cells. *PLoS One* 4, e6564 (2009).

38.   Sluder, G. & Nordberg, J. J. The good, the bad and the ugly: the practical consequences of
        centrosome amplification. *Curr. Opin. Cell Biol.* 16, 49–54 (2004).

39.   Ricke, R. M. & van Deursen, J. M. Aneuploidy in health, disease, and aging. *J. Cell Biol.*
        201, 11–21 (2013).

40.   Carter, S. L., Eklund, A. C., Kohane, I. S., Harris, L. N. & Szallasi, Z. A signature of
        chromosomal instability inferred from gene expression profiles predicts clinical outcome in
        multiple human cancers. *Nat Genet* 38, 1043–1048 (2006).

41.   Liu, L. Y. *et al.* A supervised network analysis on gene expression profiles of breast tumors
        predicts a 41-gene prognostic signature of the transcription factor MYB across molecular
        subtypes. *Comput Math Methods Med* 2014, 813067 (2014).

42.   Nikolova, V. *et al.* Carcinogenesis Advance Access published January 6, 2009 1 ©.
        Transfus. Med. 1, (2009).

43.   Khodjakov, A. & Pines, J. Centromere tension: a divisive issue. *Nat. Cell Biol.* 12, 919–923
        (2010).

44.   Pinsky, B. A. & Biggins, S. The spindle checkpoint: tension versus attachment. *Trends Cell
        Biol.* 15, 486–493 (2005).

45.   Lin, Y.-C. *et al.* Genome dynamics of the human embryonic kidney 293 lineage in response
        to cell biology manipulations. *Nat. Commun.* 5, 4767 (2014).

46.   Lilyestrom, W., Klein, M. G., Zhang, R., Joachimiak, A. & Chen, X. S. Crystal structure of
        SV40 large T-antigen bound to p53: Interplay between a viral oncoprotein and a cellular

tumor suppressor. *Genes Dev.* 20, 2373–2382 (2006).

47.   Hutton, F. G., Turnell, A. S., Gallimore, P. H. & Grand, R. J. Consequences of disruption of the interaction between p53 and the larger adenovirus early region 1B protein in adenovirus E1 transformed human cells. *Oncogene* 19, 452–62 (2000).

48.   Uetake, Y. Cell cycle progression after cleavage failure: mammalian somatic cells do not possess a 'tetraploidy checkpoint'. *J. Cell Biol.* 165, 609–615 (2004).

49.   Trachana, V., van Wely, K. H. M., Guerrero, A. A., Fütterer, A. & Martínez-A, C. Dido disruption leads to centrosome amplification and mitotic checkpoint defects compromising chromosome stability. *Proc. Natl. Acad. Sci. U. S. A.* 104, 2691–6 (2007).

50.   Chen, Y. Q. and X. Senescence Regulation by P53 Protein Family. *NIH* (2013).

51.   Beauséjour, C. M. *et al.* Reversal of human cellular senescence: Roles of the p53 and p16 pathways. *EMBO J.* 22, 4212–4222 (2003).

52.   Rufini, a, Tucci, P., Celardo, I. & Melino, G. Senescence and aging: the critical roles of p53. *Oncogene* 32, 5129–43 (2013).